Tectonophysics 509 (2011) 33–49

Contents lists available at ScienceDirect

Tectonophysics

journal homepage: www.elsevier.com/locate/tecto

Seismites in the Kathmandu basin and seismic hazard in central Himalaya

J.L. Mugnier [a,b,*], P. Huyghe [a], A.P. Gajurel [a,b], B.N. Upreti [b], F. Jouanne [a]

[a] ISTerre, CNRS, Université de Grenoble, Université de Savoie, France
[b] Department of Geology, Tribhuvan University, Ghantaghar, Kathmandu, Nepal

ARTICLE INFO

Article history:
Received 28 September 2010
Received in revised form 23 May 2011
Accepted 24 May 2011
Available online 2 June 2011

Keywords:
Himalaya
Paleo seismicity
Mega-earthquakes
Liquefaction
Soft-sediment deformation
^{14}C dating

ABSTRACT

Soft-sediment deformation structures have been analyzed at six sites of the Kathmandu valley. Microgranulometric study reveals that silty levels (60 to 80% silt) favor the development of soft-sediment deformation structures, while sandy levels (60 to 80% sand) are passively deformed. Nonetheless well sorted sand levels (more than 80% sand) generate over-fluid pressure during compaction if located beneath a silty cap, leading to fluidization and dike development. 3-D geometry of seismites indicates a very strong horizontal shearing during their development. Using a physical approach based on soil liquefaction during horizontal acceleration, we show that the fluidization zone progressively grows down-section during the shaking, but does not exactly begin at the surface. The comparison of bed-thickness and strength/depth evolution indicates three cases: i) no soft-sediment deformation occurs for thin (few centimeters) silty beds; ii) the thickness of soft-sediment deformation above sandy beds is controlled by the lithological contrast; iii) the thickness of soft-sediment deformation depends on the shaking intensity for very thick silty beds. These 3 cases are evidenced in the Kathmandu basin. We use the 30 cm-thick soft-sediment deformation level formed during the 1833 earthquake as a reference: the 1833 earthquake rupture zone extended very close to Kathmandu, inducing there MMI IX–X damages. A 90 cm-thick sediment deformation has therefore to be induced by an event greater than MMI X. From a compilation of paleo and historic seismology studies, it is found that the great (M ~ 8.1) historical earthquakes are not characteristic of the greatest earthquakes of Himalaya; hence earthquakes greater than M ~ 8.6 occurred. Kathmandu is located above one of the asperities that laterally limits the extent of mega-earthquake ruptures and two successive catastrophic events already affected Kathmandu, in 1255 located to the west of this asperity and in ~1100 to the east.

1. Introduction

The present-day tectonics of the Himalaya is characterized by under-thrusting of the Indian lithosphere along the Main Himalayan Thrust (MHT from Zhao et al., 1993; Fig. 1). Although some earthquake ruptures occur out-of sequence (Kaneda et al., 2008; Mugnier et al., 2005), most of them occur along the MHT (Avouac, 2003). Historical archives indicate that large earthquakes with >8 moment magnitude (M) have episodically ruptured several hundred kilometers long segments of the southern part of the MHT (Chandra, 1992). Several observations suggest the occurrence of mega earthquakes along the MHT (greater than the ~8.1 M historic earthquakes): a) a summation of the seismic moment for the Himalayan arc reveals that the frequency of great earthquakes during the past three centuries is insufficient to explain the transfer of the South Tibet/India convergence toward the frontal thrust belt (Bilham et al., 2001); b) trenching at the front of the belt indicates events with more than 10 m displacement (Kumar et al., 2006; Lavé et al., 2005); c) historical seismicity underlines seismic gaps (e.g. Seeber and Armbruster, 1981), the major one being located in western Nepal between the 1803 Kumaon and the 1934 Bihar–Nepal earthquakes; these gaps are potential places for very great earthquakes. The seismic hazard in Himalaya is therefore obvious, but an uncertainty remains concerning the level of destruction that could affect the Kathmandu area.

To improve the seismic hazard estimation, we have performed an extensive survey of the soft-sediment deformation and dikes preserved in the Plio–Pleistocene fluvio-lacustrine sediments of the Kathmandu Valley. The aim of this paper is to: a) perform a geometric and granulometric analysis of the soft-sediment deformation; b) propose a simplified physical approach in order to confirm that soft-sediment deformations are related to earthquake events i.e. are "seismites"; c) compare the pre-historic seismites with seismites related to well known historic events; d) propose a catalog of the great earthquakes that occurred in the Kathmandu area by taking into account our paleo-seisms study, trenching at the front of Himalaya (Kumar et al., 2006, 2010; Lavé et al., 2005) and historical earthquakes (Ambraseys and Douglas, 2004; Bilham, 1995; Chitrakar and Pandey, 1986). Finally our results are discussed using recent concepts about seismic (Avouac, 2003; Feldl and Bilham, 2006) and inter-seism behaviors (Berger et al., 2004) of the central Himalaya.

* Corresponding author at: ISTerre, Batiment les Belledonnes, Université de Savoie, F 73376, Le Bourget du Lac Cedex, France. Tel.: +33 4 79 75 86 76.
E-mail address: jean-louis.mugnier@univ-savoie.fr (J.L. Mugnier).

0040-1951/$ – see front matter © 2011 Elsevier B.V. All rights reserved.
doi:10.1016/j.tecto.2011.05.012

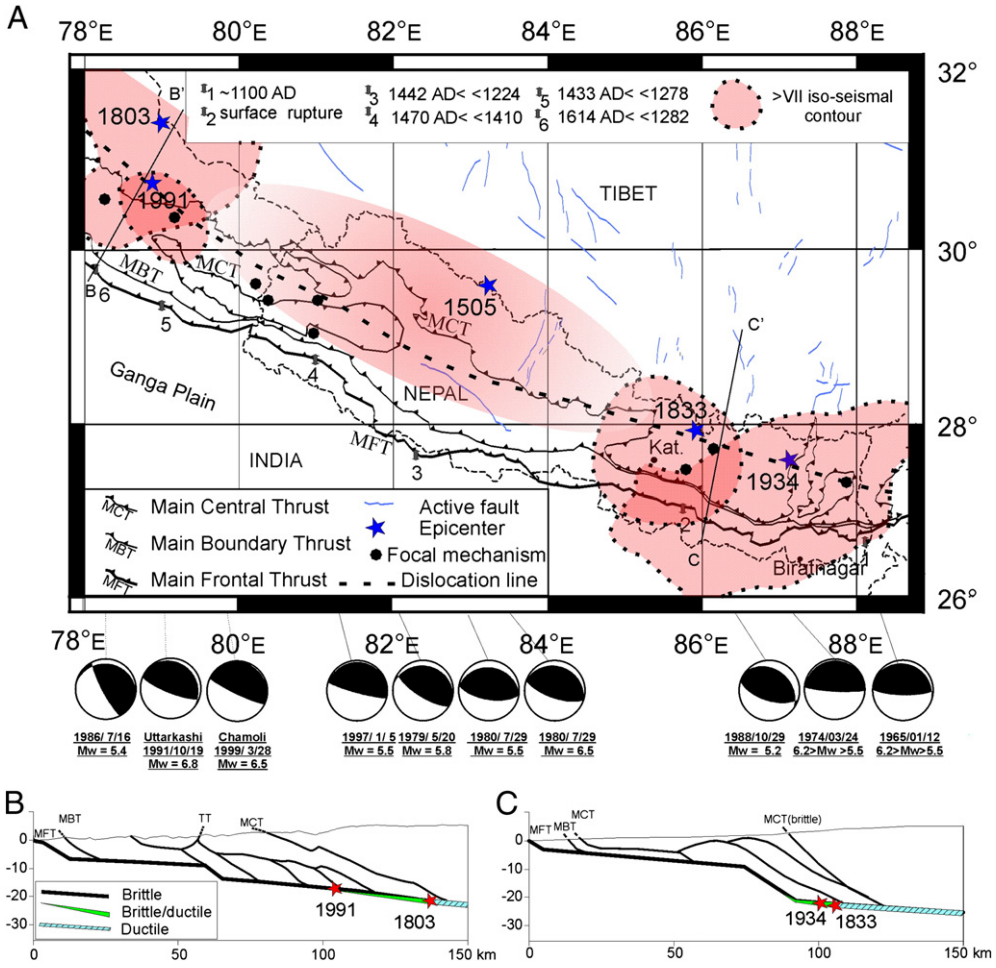

Fig. 1. A) Map of the historical great earthquakes of the central Himalaya. Kat, Jum and Nep respectively for Kathmandu, Jumla and Nepalgunj. 1934 epicenter from Chen and Molnar (1977), 1505 and 1803 epicenters from Ambraseys and Douglas (2004), 1991 epicenter from Rastogi and Shadha (1995) and IMD, 1833 event from Thapa (1997). MKS isoseismal contours for Intensity = VII from Ambraseys and Douglas (2004) for the 1934, 1803 and 1833 events and inferred from Ambraseys and Jackson (2003) for 1505 event. MMI intensity from Rastogi and Chadha (1995) for 1991 event. Location of the trenches associated to the following events: (1) ~1300 ≪ 1050 AD (Nakata, 1998), (2) ~1100 AD (Lavé et al., 2005), (3) 1442 ≪ 1224 AD (Mugnier et al., 2005 and this paper), (4) 1470 ≪ 1410 AD (Kumar et al., 2010), (5) 1433 ≪ 1278 AD (Kumar et al., 2006); (6) 1614 ≪ 1282 (Kumar et al., 2006). The focal mechanisms are from Larson (1999, CMT Harvard catalog) and from Molnar (1990) for those between 1965 and 1976. Dislocation line (~brittle–ductile transition along the MHT) adapted from Banerjee and Burgmann (2002), Berger et al. (2004) and Bettinelli et al. (2006). B) Structural cross-section of Kumaon (location on Fig. 1) adapted from Srivastava and Mitra (1994). TT: Tons Thrust. C) Structural cross-section in eastern Nepal (location on Fig. 1) adapted from Berger et al. (2004) and Schelling and Arita (1991).

2. Geological setting of the seismites of the Kathmandu basin

2.1. Structural control of great Himalayan earthquakes

The Himalaya formed by a pile of thrust sheets (Le Fort, 1975). The major thrusts (MCT for Main central thrust and MBT for Main Boundary Thrust) are presently passively displaced above the Main Himalayan Thrust (MHT). This major fault absorbs about 20 mm/yr convergence (Bilham et al., 1997). Geometry of the MHT is characterized by (e.g. Schelling and Arita, 1991) a southern frontal ramp (MFT for Main Frontal Thrust), a shallow décollement at the boundary between the Indian craton and the syn-orogenic sediments (Mugnier et al., 1999), a detachment beneath the Lesser Himalaya, a crustal ramp cutting through the crust of the Indian craton and a lower flat that extends far to the north beneath the Tibetan plateau (Fig. 1).

The crustal ramp along the MHT has been deduced from balanced cross-sections (De Celles et al., 1998; Srivastava and Mitra, 1994) and some geophysical data (e.g. Avouac, 2003; Schulte-Pelkum et al., 2005; Zhao et al., 1993) that indicate a clear difference in depth of shallow detachment beneath the external part of Himalaya and deeper detachment beneath the Higher Himalaya. This ramp is also inferred from modeling (Berger et al., 2004; Lavé and Avouac, 2001; Pandey et al., 1995; Robert et al., 2011) and it is found that the location and size of the crustal ramp vary along strike (Fig. 1B). The ramp is located to the north of the MCT surface trace in the central Nepal, whereas it is rather small and located to the south of the MCT in the western Nepal (Berger et al., 2004; Pandey et al., 1999; Robert et al., 2011).

Most of the great earthquakes occur along the MHT (Seeber and Armbruster, 1981; focal mechanisms on Fig. 1 from Larson, 1999). Some of them reach the surface along the MFT (see trench location on Fig. 1) and some along out-of sequence thrusts (Mugnier et al., 2004; Mugnier et al., 2005), like the 2005 Kashmir earthquake (Kaneda et al., 2008). However, all earthquakes do not reach the surface, like the 1991 (M~7) Uttarkashi event (Cotton et al., 1996; Rastogi and Chadha, 1995).

The ruptures of the great Himalayan earthquakes nucleate close to the brittle–ductile transition (location on Fig. 1 from Banerjee and Burgmann, 2002; Bettinelli et al., 2006) and propagate towards the Indian plain along the MHT. Lateral extent of the great earthquake ruptures is probably controlled by structural complexities that trend obliquely to the Himalayan chain. Molnar (1987) showed that lateral ramps caused the segmentation of the 1905 earthquake in several

ruptures, whereas the lateral ramps inferred at crustal scale (Berger et al., 2004; Robert et al., 2011) could affect the great ruptures of Himalaya. Strong damages occur in the external part of belt above this rupture (Avouac, 2003).

2.2. Earthquakes in the Kathmandu valley

The Kathmandu valley is located in an intermountain basin carried above the shallow flat of the MHT (Pandey et al., 1995). The basin is mostly filled by a very thick (500–600 m) sequence of fluvio-lacustrine sediments (Moribayashi and Maruo, 1980) that rests above the meta-sedimentary formations of the Lesser Himalaya (Rai, 2001). The basin geometry induces a site effect that magnifies the intensity of the earthquake damage (Dixit et al., 1998). We used the MMI (Modified Mercalli Intensity) scale proposed by Wood and Neumann (1931) for high seismic hazard estimation in the Kathmandu area in addition to the scale adapted by Ambraseys and Douglas (2004) from the Medvedev–Sponheuer–Karnik (MSK) scale and that does not consider the zones of intensity > VIII MSK.

Nepal has a long history of destructive earthquakes. At least ten major earthquakes (Chitrakar and Pandey, 1986) were recorded in the historical archives since the 13th century. The oldest event badly damaged Kathmandu in 1255 AD and the associated intensity reached at least X (Rana et al., 2007). One third of the Kathmandu population (several thousands of people), including King Abhaya Malla, was killed (e.g. Rana et al., 2007; Shava, 1992).

Between the medieval period and the 19th century only 4 events were quoted by Chitrakar and Pandey (1986) and NSET (2006). But historical record is incomplete and major events could miss. For example the 1505 AD earthquake that occurred in south-western Tibet (Fig. 1) reached a M ~ 8.2 and destroyed numerous houses close to the Tibetan border not far from the Kathmandu valley (Ambraseys and Jackson, 2003). Hence we infer some destruction in the Kathmandu valley though the 1505 event is not quoted in the historical archive of Kathmandu. A calibration of its intensity in respect to the epicenter distance (Ambraseys and Douglas, 2004) predicts MSK intensity > VI. Moreover such intensity probably magnified to MMI ≥ VII due to site effects in the valley (Dixit et al., 1998).

During the 19th century, three earthquakes induced strong destructions in the Kathmandu Valley: in 1810, 1833 and 1866 AD (Oldham, 1883). The most important one reached to M 7.6 in 1833 AD (Ambraseys and Douglas, 2004). It had been preceded by 2 foreshocks that drove people outdoors in alarm, which reduced loss of human lives though the main shock reached MMI IX–X in the Kathmandu area (Bilham, 1995); the MMI X value was assigned in the southern part of the Kathmandu basin.

The 1934 earthquake is the strongest event during the 20th century and it reached M 8.1 at the source (Ambraseys and Douglas, 2004) and induced damages with a MMI X in the Kathmandu valley (Dunn et al., 1939; Rana, 1935). Damage distribution during this event gives an estimation of the site effect and confirms that the southern part of the Kathmandu basin is affected by a strong site effect (Dixit et al., 1998; Fig. 2).

In addition to the historical events, ~1100 AD (Nepal and India) and ~1400 AD (NW Himalaya) events have been reported by trench investigations across the MFT (Kumar et al., 2006; Lavé et al., 2005) and other events are reported by seismite studies (Gajurel et al., 1998; this paper).

3. Sediment and soft-sediment deformation in the Kathmandu basin

3.1. The Kathmandu basin

The size of catchments is ~30 km in east–west direction and ~25 km in north–south direction and its outlet is through the Bagmati River (Fig. 2). A lake occupied a large part of the catchment from Pliocene to Pleistocene (Yoshida and Igarashi, 1984). The basin is filled with a very thick (500–600 m) sequence of fluvio-lacustrine sediments (Moribayashi and Maruo, 1980) and is bounded southwards by a tectonic ridge developed above the MBT. The semi-consolidated sediments consist of muds, silts, sandy loams, fine to coarse sands and gravel to pebble conglomerates (Katel et al., 1996). The sedimentary facies (Sakai et al., 2001, 2006) are related to delta plain, delta front and pro-delta environments. Numerous fluctuations of the lake level have been recognized (Gajurel, 2006) and the classical nomenclature (Fig. 2 adapted from Yoshida and Gautam,

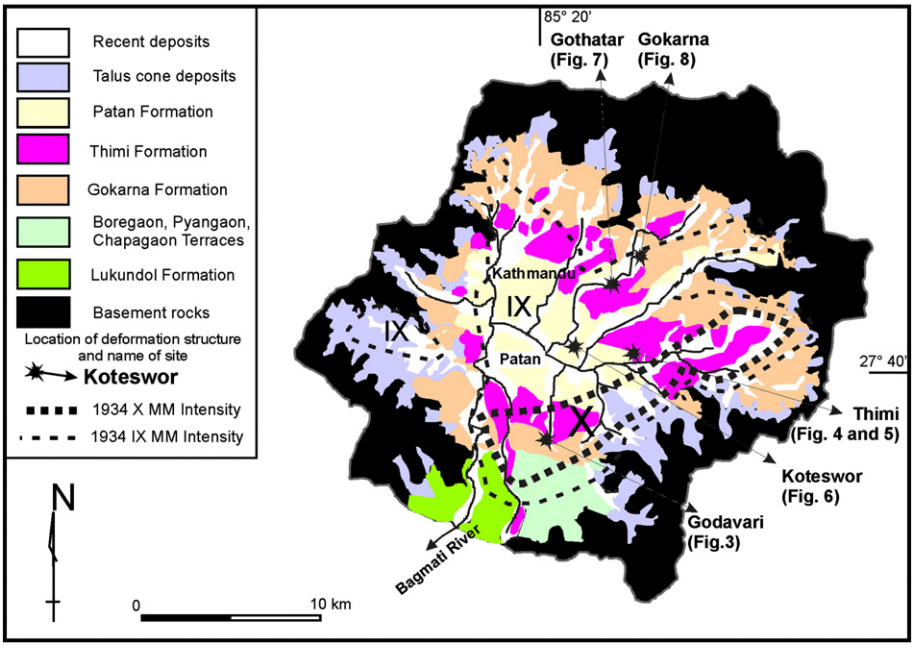

Fig. 2. Geological map (adapted from Yoshida and Gautam, 1988) of Kathmandu hydrological catchment with location of paleo-seismites (Table 1). Iso-intensity distribution of the 1934 earthquake from Dixit et al. (1998).

1988) is mainly related to terraces at the top of deltas developed during different stages of the lake extension (Sakai et al., 2006): the Lukendhol and Boregaon-Pyangaon-Chapagaon formations were deposited between 2.8 and 1 Ma during the older stages of the lake development; the Gokarna formations are related to several stages of the lake development between 1 Ma and 29 kyr (Gautam et al., 2001); the Thimi formation was deposited between ~29 and 19 kyr BP (Yoshida and Igarashi, 1984); the Patan formation is associated to the last stage (19–11 kyr). Outlet of the paleo-lake took place ~10 kyr ago and was followed by river incision resulting in the development of several recent fluvial terraces (Yoshida and Gautam, 1988).

The mineral composition of the Kathmandu basin has been intensively studied thanks to drill-wells (Fujii et al., 2001). In the 50 m upper deposits, the sediment composition shows a rapid up-section decrease in mica (40% to 14%) and a simultaneous increase in quartz (20% to 44%) and feldspar (20% to 32%). Chlorite, kaolinite and smectite minerals gradually increase up section (Fujii et al., 2001; Gajurel, 2006). Nonetheless, the smectite proportion is always less than 10% and usually less than 5%; the sum of chlorite and kaolinite proportions is always less than 15% and usually less than 10%.

3.2. Soft-sediment deformation in the Kathmandu basin

3.2.1. Presentation

During several years, fresh outcrops in sand quarries, building foundations and trenches have been analyzed in the Kathmandu basin (Gajurel, 2006). Numerous soft-sediment deformation structures have been observed in the weakly consolidated Pleistocene delta plain deposits or in the flood plain of the Bagmati River. Two types of structures occurred in the sediments of the Kathmandu basin: a) dikes were fed by liquefied sands (Obermeier, 1996) and formed sub aerial cones when they reached the surface; dikes observed in the valley of Kathmandu are thin compared to classical examples of dikes described in America by Obermeier (1996); b) soft-sediment deformation features affected the top of the sedimentary pile and completely de-organized the initial tabular attitude of sediments, leading to ball-and-pillow, flame and folded structures.

Development of soft-sediment features implies poorly consolidated silt sediment in a fully water-saturated environment, but determining the cause of soft-sediment mobilization remains a major problem: possible triggers include earthquakes (Obermeier et al., 2002), sediment loading (Moretti and Sabato, 2007), disturbance due to movement on a near-surface gravity slide (Beck, 2009), wave action (Owen and Moretti, 2008), ice sheet influence (Menzies, 2002) and gas expulsion or over-fluid pressure during fast sedimentation (Malkawi and Alawneh, 2000). Furthermore, soft-sediment deformation and dikes may be a direct or a secondary effect of earthquakes (Seilacher, 1991). We have performed a detailed study based on geometry, granulometry and dating of the structures in the Kathmandu basin. We describe in the following paragraphs six soft-sediment deformation sites (Fig. 2) among the 12 studied sites in order to discuss the processes involved during their development.

3.2.2. Methodology

3.2.2.1. Geometric study. Geometric study combining structural and sedimentological analysis has been performed. The cleaned exposures were divided into $20\times20\ cm^2$ cells using nail and string. 2-D geometries of the structures were logged in graph papers. Detailed sedimentological studies of sediment have been performed in and around the sites of soft-sediment deformation. In some cases, progressive scrapping of the semi-consolidated sediment was made to observe 3-D geometry and construct serial cross-sections.

3.2.2.2. Granulometric analysis. Granulometric analysis of the <1 mm fraction was performed by laser diffraction using the Malvern particle-size model 215 FR at the University of Savoie (France). The following classes were considered: clay (fraction<4 μm), silt (4–64 μm) and sand (fraction>64 μm).

3.2.2.3. Dating. The development of deformation features was dated using ^{14}C. We collected peat sample or organic matter to obtain a ^{14}C age close to the age of the deposited sediment (Tables 1, 2, 3). ^{14}C measurements were carried out at the Poznań Radiocarbon Laboratory (Poland), Oxford laboratory (England) or Arizona laboratory (USA) by AMS techniques and at Lyon (France) by conventional method. ^{14}C ages lower than ~21.5 ^{14}C kyr were calibrated using the CALIB program version 5.0 (Stuiver et al., 1998), based on the IntCal04 data set (Reimer et al., 2004) and intercept ages with 1σ and 2σ confidence level are reported (Tables 2 and 3). Calibrated ages in the text (Cal AD or BC) are given as the time interval linked to the highest 1σ related probability.

3.3. Soft-sediment deformation and dike developments at Godawari site

The Godawari site (Fig. 3) is located in the southern part of the Kathmandu valley, in delta deposits of the paleo-lake.

Table 1
^{14}C dating in the Kathmandu basin.

Location	Depth beneath top of the terrace (m)	^{14}C age (yr)	Uncertainty	Laboratory code	Sample number	Sample type	Sampling date	Method	Reference
Gokarna	0.52	105	34	AA-50066	Bag 2	Plant debris	2002	AMS	Gajurel(2006)
Gothatar	0.4	133	34	AA-50061	Go 2	Plant debris	2002	AMS	Gajurel(2006)
Gothatar	0.6	40 900	1400	AA-50060	Go 1	Charcoal[a]	2002	AMS	Gajurel(2006)
Koteswor	?	11 070	290	Gak-6201	?	?	?	Conventional	Yonechi(1976)
Koteswor	?	13 140	380	Gak-6200	?	?	?	Conventional	Yonechi(1976)
Thimi	32	38 265	1230	Ly-9342	Timi KTM4	Wood[a]	1997	Conventional	Gajurel(2006)
Thimi	28.7	29 290	1390	Ly-11189	00.74	Bark[a]	2000	Conventional	Gajurel(2006)
Thimi	26	45 140	1310	Lyon-509 (Oxa)	Th 3	Charcoal[a]	1997	Conventional	Gajurel(2006)
Thimi	25.8	21 650	250	Lyon-1957(Poz)	00.60	Wood	2000	Conventional	Gajurel(2006)
Thimi	19.5	41 700	5600/3200	VRI-1980	?	?[a]	?	Conventional	Paudayal and Ferguson(2004)
Thimi	13.7	36 270	930	AA-50056	NTH10	Charcoal[a]	2002	AMS	Gajurel(2006)
Thimi	12.5	43 180	1160	Lyon-508(Oxa)	Th2	Charcoal[a]	1997	Conventional	Gajurel(2006)
Thimi	12	>37000		VRI-1979	?	?[a]	?	Conventional	Paudayal and Ferguson(2004)
Thimi	7.2	33 860	610	AA-50057	ThS1C1	Charcoal	2002	AMS	Gajurel(2006)
Banyatar	13.5	>49900		AA-50059	Car D9	Charcoal[a]	2002	AMS	Gajurel(2006)
Banyatar	16.5	48 700	3700	AA-50058	Car D6	Charcoal[a]	2002	AMS	Gajurel(2006)
Banyatar	33	40 000	1300	AA-50062	Bishnu Car2	Lignite	2002	AMS	Gajurel(2006)

[a] Reworked.

Table 2
Calibrated age of the charcoals of Bagmati River and Koteswor (Calib14 program, Stuiver et al., 1998; calibration data set: intcal04.14c from Reimer et al., 2004).

Sample	Radio-carbon age BP	Calibrated age 1σ Ranges: [start:end]	Relative area under probability	Calibrated age 2σ ranges: [start:end]	Relative area under probability
Gokarna Bag 2	105 ± 34	[Cal AD 1693:1727]	0.27	[Cal AD 1681:1739]	0.27
N 7°43.944′		[Cal AD 1812:1893]	0.62	[Cal AD 1744:1763]	0.02
E 85°23.122′		[Cal AD 1906:1919]	0.09	[Cal AD 1802:1938]	0.68
Labcode AA-50066					
Gothatar Go 2	133 ± 34	[Cal AD 1681:1706]	0.16	[Cal AD 1670: 1779]	0.42
N 27°42.892′		[Cal AD 1719:1739]	0.12	[Cal AD 1799:1893]	0.41
E 85°22.489′		[Cal AD 1745:1746]	0.01	[Cal AD 1905:1943]	0.15
Labcode AA-50061		[Cal AD 1751:1762]	0.06		
		[Cal AD 1802:1819]	0.11		
		[Cal AD 1832:1883]	0.33		
		[Cal AD 1914:1938]	0.16		
Koteswor 1 Labcode Gak-6201	11070 ± 290	[Cal BC 11331:10849]	1.00	[Cal BC 11676:10415]	1.00
Koteswor 2 Labcode Gak-6200	13140 ± 380	[Cal BC 14173–13078]	1.00	[Cal BC 14642–12316]	1.00

3.3.1. Geometry and timing of the dike development

Four dikes and one soft-sediment deformation are observed at the same exposure. Soft-sediment deformation is observed within the upper unit (d on Fig. 3A), composed of silts and relics of disturbed sandy layers. Dike 3 extends upward more than 2 m from its liquefied sandy source (unit a) to the paleo-surface where it built a cone, latter overlain by deposits (unit f). Three other dikes have a common source (unit b) that is shallower than the source of dike-3. Dike-1 also built a cone on the surface of the delta plain, whereas dikes-2 and 2bis did not reach the paleo-surface.

Orientation of the dikes strikes N 355°E to N 10°E, perpendicular to the N 100°E paleo-shore line (Yoshida and Gautam, 1988) and 20° apart from the mean paleo-flow direction. Therefore, orientation of these dikes is not coherent with a horizontal stretching due to lateral spreading or flow effects.

The cross-cutting relations between dikes and host sediments allow establishing a relative timing of deformation. Soft-sediment deformation in the upper layers (unit d) induced a folding of dike-1 and therefore occurred after dike-1 development. Soft-sediment deformation is cross-cut by linear dikes-2 and 3, hence deformation occurred prior them. The soft-sediment deformation that affected the upper level probably occurred during the liquefaction of the source level (unit b) of dikes-1 and 2 because dike-1 was affected by the upper deformation structure whereas dike-2 cuts through it. Dike-3 cuts through the source bed (unit b) of dikes-1, 2 and 2bis, hence it occurred after their formation. Nonetheless, at the time scale of the sedimentary record, all these deformations occurred simultaneously because the cones built by dikes-1 and 3 laid upon the same paleo-surface.

3.3.2. Granulometry of the dike and host material

A granulometric study of soft-sediment deformation levels, dike-1, source bed and host levels has been performed. It shows that (Fig. 3B): a) soft-sediment deformation (level d) is characterized by a large component of silt, whereas source (level b) and dike filling material are rich in sand; b) the dike is not homogeneous; the sand proportion decreases regularly from 75% close to the source to less than 20% in the cone and the clay proportion increases from less than 5% in the source level to more than 25% in the cone; c) the same depth variation of the granulometry occurs for the host sediment and the contrast between granulometry of the dike and the host sediment is weak. We suggest that these variations of dike granulometry are mainly due to assimilation of host material within the dike and to very little u-section transport of the source material. The term assimilation is used when the host at the vicinity of the dike is disaggregated by liquefaction, leading to an increase of the dike thickness. The assimilation assumption is also supported by direct observations: a) in numerous zones, the transition between the dike and the border is

Table 3
Calibrated age of the charcoals of Koilabas River (Calib14 program, Stuiver et al., 1998; calibration data set: intcal04.14c from Reimer et al., 2004).

Sample	Radio-carbon Age BP	Calibrated age 1σ Ranges: [start:end]	Relative area under probability	Calibrated age 2σ Ranges: [start:end]	Relative area under probability
Koilabas 00–09	515 ± 45	[Cal AD 1332–1337]	0.05	[Cal AD 1311–1359]	0.23
N27°41.46′		[Cal AD 1398–1442]	0.94	[Cal AD 1387–1451]	0.76
E082°31.6690′					
Labcode Lyon-1816(GrA-20805)					
Koilabas 00–20	775 ± 35	[Cal AD 1225–1271]	1.00	[Cal AD 1190–1196]	0.01
N27°41.22′				[Cal AD 1207–1285]	0.99
E82°31.57′					
Labcode Poz AA-50070					
Koilabas 00–15	180 ± 30	[Cal AD 1666–1683]	0.18	[Cal AD 1653–1695]	0.20
N27°41.22′		[Cal AD 1735–1783]	0.52	[Cal AD 1726–1814]	0.56
E82°31.57′		[Cal AD 1796–1805]	0.10	[Cal AD 1837–1844]	0.01
Labcode Poz-22643		[Cal AD 1933–1951]	0.20	[Cal AD 1851–1869]	0.02
				[Cal AD 1872–1876]	0.01
				[Cal AD 1917–1952]	0.20
Koilabas 00–16	132 ± 34	[Cal AD 1681–1707]	0.17	[Cal AD 1670–1779]	0.42
N27°41.23′		[Cal AD 1719–1738]	0.12	[Cal AD 1799–1894]	0.42
E82°31.67′		[Cal AD 1754–1762]	0.05	[Cal AD 1905–1943]	0.15
Labcode AA-50068		[Cal AD 1802–1825]	0.13	[Cal AD 1950–1953]	0.01
		[Cal AD 1832–1885]	0.36		
		[Cal AD 1913–1937]	0.16		
		[Cal AD 1951–1952]	0.01		

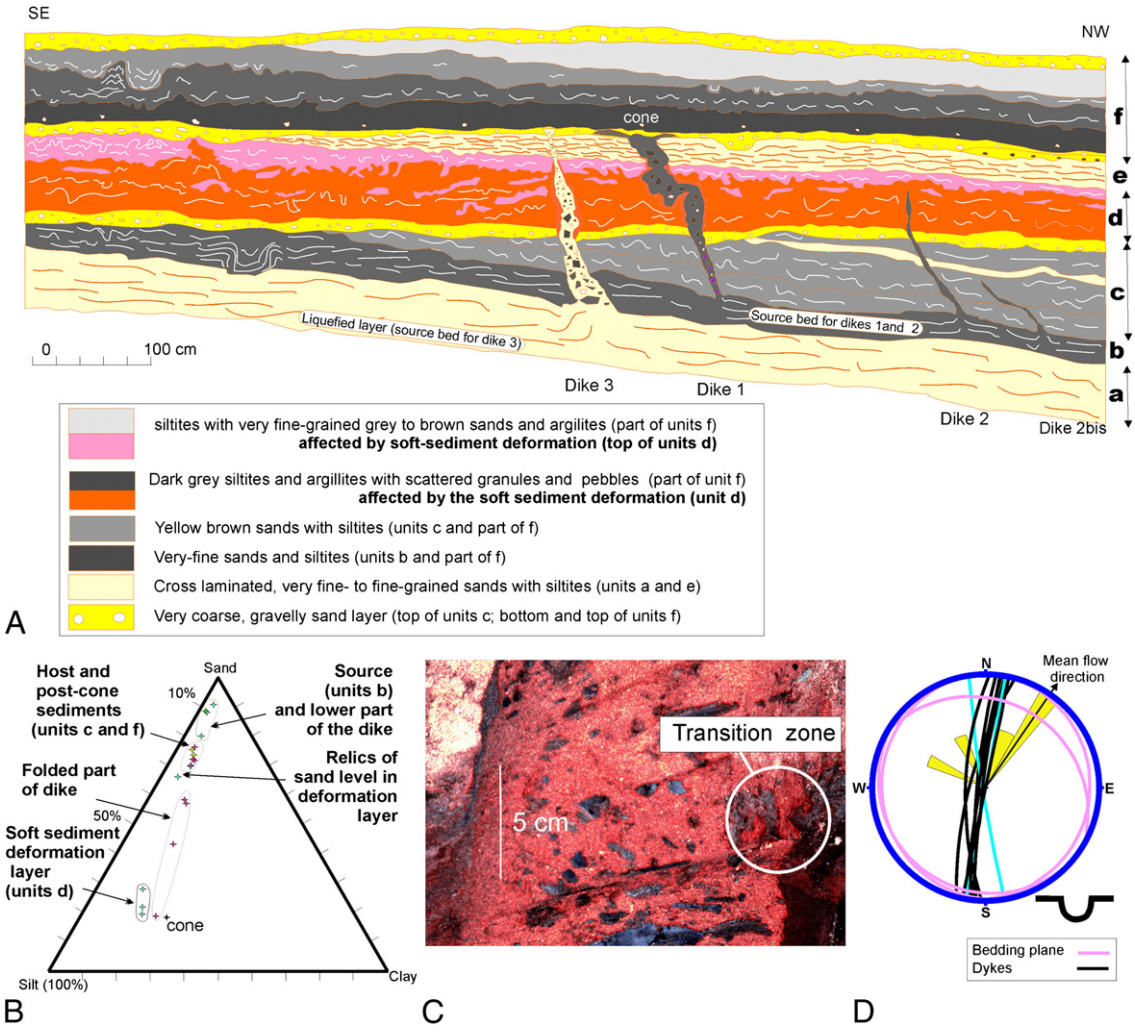

Fig. 3. A) Dikes and soft-sediment deformation at Godawari. (a) to (f) refer to different units; the pink and brown unit (d) refers to the soft-sediment deformation features; B) granulometric analysis of soft-sediment deformation layer, dike 1 and source and host of the dike; C) photography of clasts and borders of the dike; D) orientation of dikes, bedding plane and current flow direction.

not a surface but rather a diffuse zone; b) numerous clasts within the filling of the dike are relics of the host sediment (Fig. 3C). The relics show strong rotations – as great as 90° – but are either weakly upraised or descended in the dikes. These motions indicate that there was few up-section particle transport and possibly transversal transport (Levi et al., 2006). The small size of the cones also agrees with a weak alimentation and therefore a small up-section transport .

3.4. Geometry of the soft-sediment deformation at Thimi site

3.4.1. Site description

The site is located in the sand quarry of the Thimi village (Fig. 4). Numerous soft-sediment deformation levels are observed along an outcrop more than 33 m high and with a more than 50000 m^2 horizontal extension (Gajurel et al., 1998). Height distinct soft-sediment deformation stratigraphic horizons were observed at Thimi. The age of the sediment extends from ~19 kyr BP at the top of the Thimi formation from ^{14}C ages (Sakai et al., 2001) to ~42 kyr BP at the base from paleo-magnetic study (Gautam et al., 2001). The Thimi formation developed in a delta front environment that prevented small particles of organic matter to be preserved. Therefore we collected big wood pieces and charcoals, but seven over nine ^{14}C ages are not in a stratigraphic order and were remobilized. This result keeps it impossible to estimate the recurrence of the seismites and suggests that most of the delta front sediments are reworked from older sediments deposited in a more extended lake (Table 1). Nonetheless the 2 ages that are in a stratigraphic order confirm that the Thimi formation Sensus Stricto is superposed above the Gokarna formation (Gajurel, 2006) in the studied site. The boundary between the Thimi and Gokarna formations is clearly expressed along an erosion surface. Among the 8 seismites levels, we describe a continuous level of pillow dated at ^{14}C 29290 ± 1390 yr and a complex soft-sediment deformation dated at ~42 kyr BP (Gautam et al., 2001).

3.4.2. Lateral evolution of single ball-and-pillow level

A soft-sediment deformation affected a succession of centimeter thick cross-laminated sandy and silty layers. It is found down-section (Fig. 4A): an undeformed silty level (sample '68'); an unconformity at the top of a homogeneous but strongly deformed silty material (sample '61') around the pillow; the sandy pillow (sample '62'); the strongly deformed silty material (sample '63'); a succession of undeformed sandy levels (samples '64', '65', '66'); and an undeformed silty level (sample '67'). The granulometry of the strongly deformed silty material is similar to those of the above or underneath undeformed level, with ~64% silt, 29% sand and 7% clay (Fig. 4B),

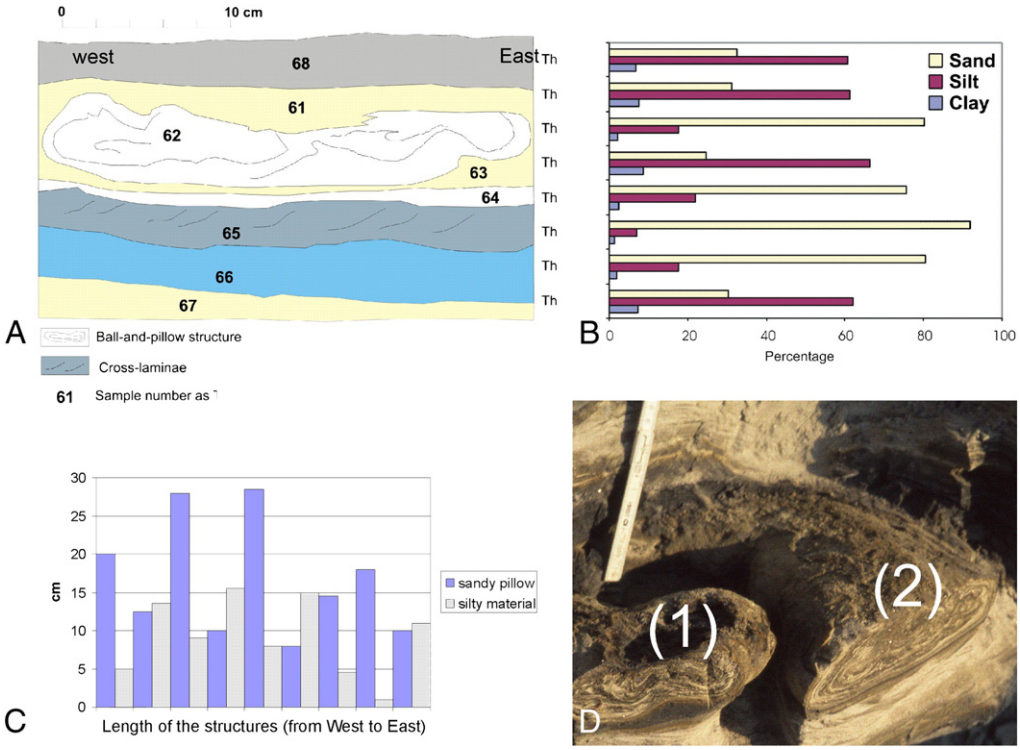

Fig. 4. A simple soft-sediment deformation level at Thimi. A) geometry of a pillow in a vertical cross-section with location of samples used for granulometry; B) sand, silt and clay proportions; sample '62' is related to pillow, '61' and '63' to fluidized matrix and '65' to '68' to undeformed cross-laminae levels (see location on Fig. 3A); C) successive horizontal width of the sandy pillows (heavy gray) and of the silty fluidized zone (lightgray) on a vertical cross-section; D) 3D view of pillows: pillows 1 and 2 appear distinct in a single cross-section, but are two sections of a same curved bolster when silty fluidized material is removed.

whereas the composition of pillows is similar to the composition of the undeformed sandy level that bounds downward the soft-sediment deformation, with ~80% sand and 20% silt.

The studied level shows a regular succession of different layers, but a lateral evolution is observed along a distance of ~40 m for the layers containing the samples '61', '62' and '63': the total thickness of these layers decreases regularly westward, and soft-sediment deformation laterally ends when the total thickness is smaller than 5 cm.

In a cross-section, horizontal length of the pillows (Fig. 4C) varies between 10 and 25 cm and the pillows are separated by thin zones of deformed silty material (15 to less than 5 cm). The length scattering of the horizontal separation and extent of the pillows in 2D outline the absence of a structural periodicity, whereas the 3D geometry (Fig. 4D) shows that pillows are connected to each other and formed curved bolsters. The syncline-like geometry of pillows suggests that silty material intruded upward within the sandy level.

3.4.3. Superposed soft-sediment deformations

Several unconformities are observed in the 35 cm thick soft-sediment deformation layer dated at ~42 kyr. The highest unconformity (Uc0) (Fig. 5A) locates above the soft-sediment deformation. Thin alternating sand and silt layers show clear onlap westwards and eastwards above the unconformity 'Uc1' (Fig. 5A), suggesting that it was gently folded. A lower boundary 'Uc2' (Fig. 5A) is strongly folded. We interpret it as an unconformity because it linearly cuts through (left side of Fig. 5A) and therefore post-dates the underneath pillow structures. Nonetheless the strong deformation prevents us to definitively recognize the unconformity character from sedimentological criteria. A general cartoon depicting soft-sediment deformation development is suggested in Fig. 5B. The stratigraphic unconformity 'Uc2' formed after a first shaking that affected the sediment located beneath the unconformity and was folded during a second shaking that affected the soft sediment located above it. The unconformity was folded because the thickness of the deformation zone during this shaking was greater than the thickness of the sediment deposited between the 2 shaking events. Therefore, the sediment located beneath the unconformity 'Uc2' suffered two successive shaking events and their mechanical properties did not significantly change between the two events. Nonetheless, unconformity-like surfaces occurred during the experiments of Moretti et al. (1999) and the final configuration could also be explained if the lower deformed beds were more susceptible to liquefaction.

3.5. Mega soft-sediment deformation at Koteswor

3.5.1. General description

This soft-sediment deformation level is the thickest one observed in the Kathmandu valley. The Koteswor site was located in the pro-delta sediment of the Patan formation (Sakai et al., 2001). Age of the soft-sediment deformation level is between Cal BC 14 173 yr and Cal BC 10 415 yr from two ^{14}C dating (Table 2) respectively obtained in the upper and lower parts of the Koteswor outcrop (Yonechi, 1976). The detailed study of the Koteswor soft-sediment deformation can be found in Gajurel et al. (2000) and we remind here the main characteristics (Fig. 6).

The underlying undeformed layers are composed of very fine grained sand cross-laminated ripples, and 3 to 6 cm thick alternating sequences of inversely graded and thinly laminated argillite and siltite. The thickness of the deformed layer is 70 to 90 cm. It consists from top to bottom: (a) a homogenized zone composed of elutriated particles, (b) a ball-and-pillow zone that is intensely folded; the matrix around the ball-and-pillow zone is composed of sandy silt with less than 7% of clay and the ball-and-pillow structures are composed of thinly laminated sand with less than 20% of silt and clay (Gajurel et

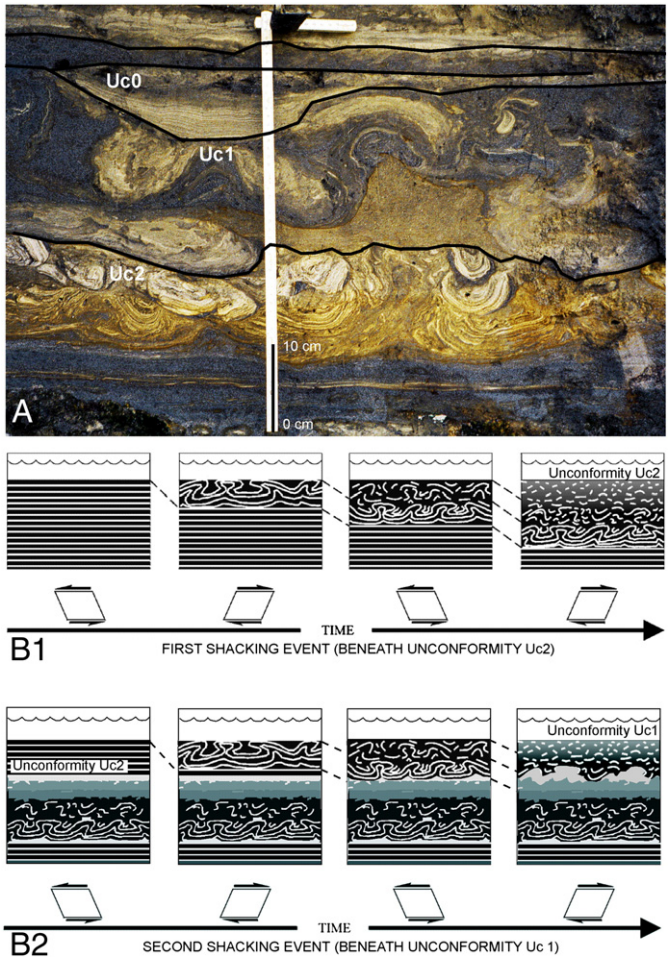

Fig. 5. A) A complex geometry of the soft-sediment deformation horizon at Thimi (~42 kyr BP); (Uc0) is the unconformity at the top of a soft-sediment deformation level. The unconformity (Uc1) is gently folded after or during the deposition of thinly laminated beds; (Uc2) is a strongly folded unconformity within the soft-sediment deformation structure; B) a cartoon illustrating two successive soft sediment deformation events separated by a phase of sedimentation; B1) deformation of the older sediments (beneath unconformity Uc2) during a first shaking event (adapted from Rodriguez-Pascua et al., 2003); B2) sedimentation occurs above unconformity Uc2, followed by development of a soft sediment deformation during a second shaking event that affects the sediment deposited above and beneath unconformity Uc2 and strongly folded unconformity Uc2.

al., 2000), and (c) a lower zone which is moderately folded with continuous sandy layers embedded in deformed sandy silt.

3.5.2. 3D geometry of the pillows

3D images of ball-and-pillow structures have been obtained by progressive scrapping of semi-consolidated sediment and realization of serial cross-sections. Fig. 6B shows four successive cross-sections, respectively at 0, 8, 17 and 27 cm behind each other. In the cross-section-4, three pillows are observed whereas in the cross-section-3, the left and right pillows of cross-section-4 are connected by a continuous and stretched sand level and the central pillow of cross-section-4 thrusts over the two connected pillows. This central pillow also thrusts above the other pillows of cross-sections-2 and 1, suggesting a several tens cm horizontal displacement. The cross-section-3 clearly illustrates that horizontal stretching and vertical thinning are the causes for dividing of pillows. This 3D geometry excludes a simple vertical expulsion of fluidized sediment to explain the dividing of pillows and suggests a succession of stretching and shortening episodes that led to displacement of the upper part in respect to the lower part.

3.6. Soft-sediment deformation affecting the recent deposits of the Bagmati River

Due to sand extraction, a very recent incision occurs within the deposit of the Bagmati River and soft-sediment deformation is observed at Gothatar and Gokarna sites (Fig. 2, Gajurel et al., 2002). Bricks are found in the deposits of these two sites attesting to their recent age. ^{14}C dating of 2 charcoal samples in the soft-sediment deformation layer at Gothatar (Fig. 7) has respectively ascertained the dates of 133 ± 34 ^{14}C yr and $40\,900 \pm 1400$ ^{14}C yr; the second age refers to reworked sediment of the Gokarna formation. A charcoal from the flame structures of Gokarna has been dated at 105 ± 34 ^{14}C yr (Fig. 8).

3.6.1. The Gothatar site

Two types of structures are found in the left bank of the Bagmati River at Gothatar (Fig. 7A).

In the lower part of the outcrop, three sand dikes cut through a succession of undeformed layers. These dikes tip upward in undeformed layers and are connected to the underneath coarse sand layer that is their source as evidenced by the similar granulometry (Fig. 7C). The source was only partly liquefied; preserved sedimentary features indicate a channel and point bar depositional environment leading to a high porosity. The strike of dikes lies between N 150°E and N 165°E (Fig. 7D) and is oblique to the NNE to SSW direction of the present-day Bagmati River and local relief. This obliquity excludes a lateral spreading origin.

In the upper part of the outcrop, soft-sediment deformation affects a ~30 cm-thick silty unit (Fig. 7D) in which the granulometry is similar to that of the underneath undeformed layers (Fig. 7C). Sandy lenses in the soft-sediment deformation zone have the same granulometry as that of the sandier undeformed layers and hence are relics of sandy layers that were disrupted by deformation.

The source level of the sand dikes is formed of well-sorted material (~85% sand, ~12% silt and less than 4% clay), the host of the dikes and the soft-sediment deformation levels are formed of poorly sorted silt (~28% sand, ~60% silt and ~12% clay). Few less than 2 cm thick layers are sandier.

3.6.2. The Gokarna site

The outcrop is located on the right bank of the low flow channel of the Bagmati River, extending laterally more than 20 m (Fig. 8). The soft-sediment deformation consists of flame structures within silty layers and contorted sandy layers. The interface between silt and sand levels is folded, but sand injections locally occurred within silt. The folded structures are rather symmetric and when they are asymmetric, their orientation is not in agreement with a dragging effect at the base of the present-day Bagmati River that flows here from North to South. The soft-sediment deformation is covered by a 30 cm thick very young soil where no horizon has yet developed.

3.6.3. Thickness of the Bagmati soft-sediment deformation levels

At Gothatar, the granulometric similarity between undeformed (star on Fig. 7C) and 30 cm-thick deformed layers (dot on Fig. 7C) suggests that the base of the deformed level is not controlled by granulometry. At Gokarna, the thickness of the soft-sediment deformation level is 35–40 cm where sand injections are incorporated at its base, but is only 30–35 cm where deformed silty layers lie above undeformed silty layers. We therefore consider that the soft-sediment features of Gokarna and Gothatar have a similar thickness of ~30 cm.

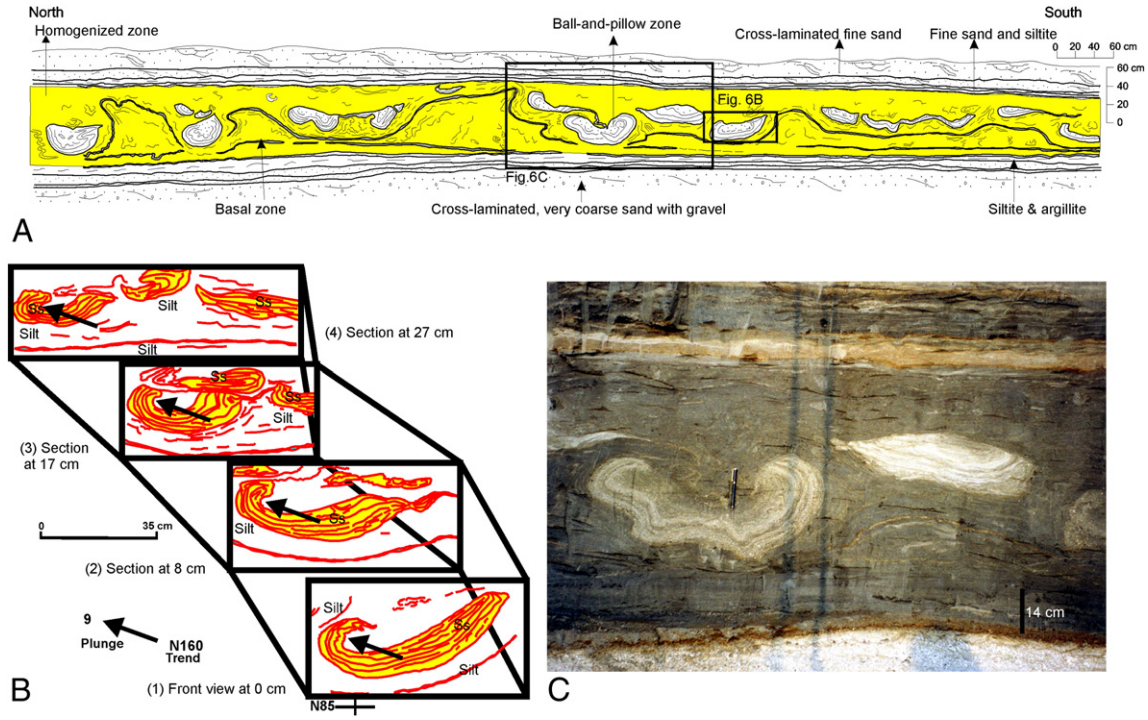

Fig. 6. A) Cross section of the Koteswor seismite zone (from Gajurel et al., 2000); B) serial cross-sections of a ball-and-pillow structure (location on Fig. 6A) (Ss for silty sand); C) and D) photographs of ball-and-pillows (location on Fig. 6A).

4. Discussion

4.1. Characteristics of the soft-sediment deformation in the Kathmandu basin

4.1.1. Soft-sediment deformation and fluidization of the silt levels

All the observed ball-and-pillows (Koteswor and Thimi sites; Figs. 4, 6) are characterized by the same granulometric contrast between the sandy pillows and the silty matrix, although their thickness and geometry are quite different. The geometry in all cases indicates a fluidization of silty levels during the development of soft-sediment deformation but does not argue for liquefaction of sand layers: the sand layers are rather passive markers.

The thickness of the soft-sediment deformation is limited by a contrast in lithology at the base of the silty level at Thimi (Fig. 4) and Koteswor (Fig. 6). Further, the soft-sediment deformation level at Thimi (Fig. 4) reflects a strong fluidization of silt layers but tips laterally if the silty level is too thin.

The ~42 kyr old example at Thimi (Fig. 5) outlines that thickness of a soft-sediment deformation units does not necessarily reflect the

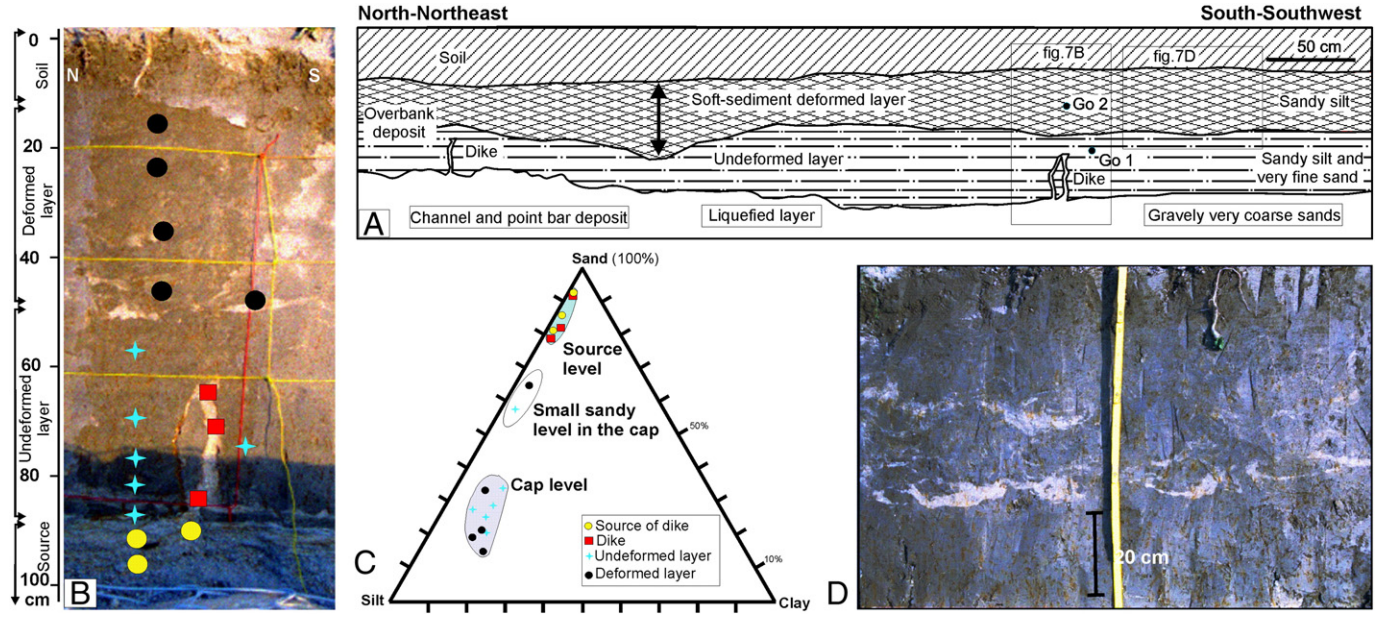

Fig. 7. Seismites in the sediments of the Bagmati River at Gothatar. A) Trench cross-section and location of samples for ^{14}C dating; B) location of samples used for the granulometric study; C) proportion of sand, silt and clay; D) a detail of flame structures in the deformed zone.

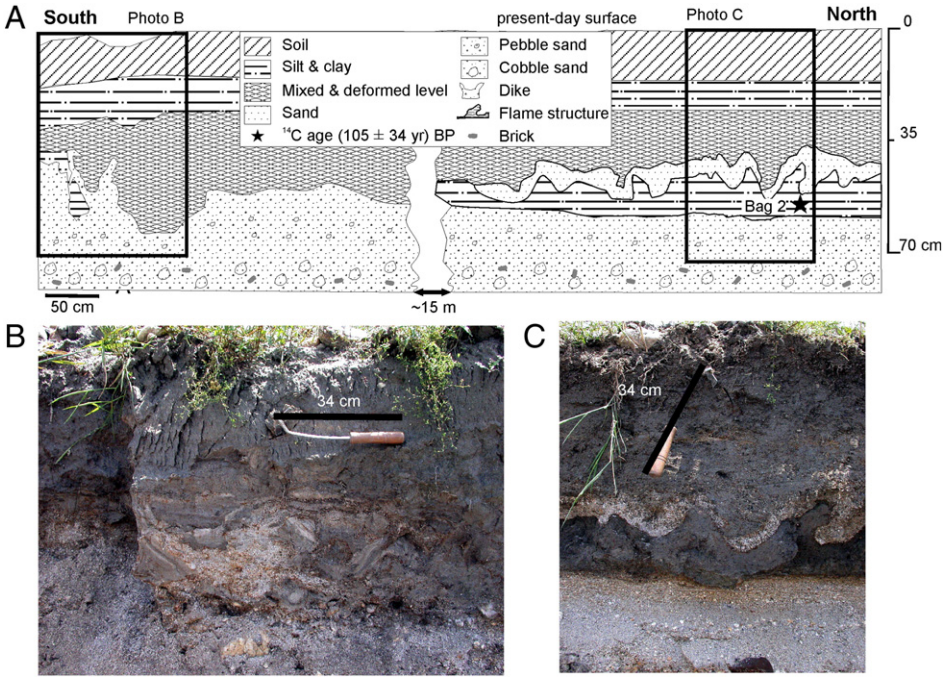

Fig. 8. A) Sketch of the 1833 AD soft deformation feature in the recent terrace deposits of the Bagmati River at Gokarna village; thick rectangles show location of pictures; B) sand injection in the deformed level and C) contorted sand layers.

intensity of a single shaking event and can be related to the superposition of several events. This implies that a silty soft-sediment layer could be deformed by several successive events separated by phases of overlying sedimentation as long as silty sediment remains water-saturated and no induration occurs.

4.1.2. Association of dyke and soft-sediment deformation levels

The structures of the Godawari site (Fig. 3) outline that dike development both involves fracturing in an environment of strong fluid pressure and assimilation of the host sediments at the border of the dike. Combination of these two processes indicates high fluid pressure and a weak fluid pressure contrast between the dike and the host. Furthermore, soft-sediment deformation and dikes occurred simultaneously. This association is not inferred in the case of slump features and hence suggests a regional shaking as the unique cause of the different structures.

4.1.3. Soft-sediment deformation and historical earthquakes

During the last millennium covered by the historical archives of earthquakes, the sedimentary record is very poor and discontinuous due to the fluvial character of the sedimentation. Nonetheless, the structures of the Bagmati River have been dated using ^{14}C method (see Section 3.6). The strongest probability intervals (Reimer et al., 2004) respectively are set between Cal AD 1832 and 1883 and between Cal AD 1812 and 1893 for two samples (Table 2).

This time periods include the 1833 AD and 1866 AD earthquakes that affected the Kathmandu Valley (Chitrakar and Pandey, 1986). The 1866 events did not exceed MMI VIII (Chandra, 1992; Oldham, 1917) whereas the 1833 earthquake reached locally up to X in the Kathmandu Valley (Bilham, 1995). The May 23rd 1866 event occurred before the period of high stand river levels, hence is unfavorable for soft-sediment deformation development and can be ruled out. On the contrary the 1833 earthquake occurred on August 26th during monsoon season and the river flowed above the soft sediment deformation sites. We therefore propose that Bagmati soft-sediment deformation structures are related to the 1833 earthquake.

4.1.4. Links between the geometry and the trigger of soft-sediment deformation

The internal geometry of structures and their orientation in respect to their geomorphologic context have been investigated. It has been checked in all sites that there is no link between orientation of dikes and local paleo-slopes in order to preclude gravity structures due to sliding towards a delta front or lateral spreading towards the border of a terrace riser. It has also been checked that there is no evidence of asymmetry or any other sedimentological criteria in favor of slumping or flooding during the development of soft-sediment deformation.

The Koteswor site both outlines shortening, extension and shearing in planes parallel to the surface during the development of soft-sediment deformation. We relate the development of this soft-sediment deformation to seismic waves inducing alternate shearing between planes parallel to the earth surface. Such a shearing could be related to the Love waves or horizontal component of the Rayleigh waves (Heifetz et al., 2005; Rodriguez-Pascua et al., 2003).

4.2. A context favorable to seismites development

On one hand, the geomorphologic context of Kathmandu basin is not favorable to the development of dikes and soft-sediment deformation features by glacial, gravity or over-fluid pressure origins for the following reasons: a) the elevation of the Kathmandu basin is ~1300 m and the highest altitude in its hydrologic catchments is 2765 m, preventing the occurrence of glaciers even during the Quaternary glaciations (Gayer et al., 2006), when the equilibrium-line-altitude of ice was close to 2500 m; b) rock avalanches or landslides are not reported in the mountains close to the margin of the paleo-Kathmandu lake; c) more than half of the water shed was occupied by the paleo-lake and the lacustrine terraces are constituted by a succession of small deltas related to small rivers; d) the Kathmandu paleo-lake was shallow and gentle sub-marine slopes were not favorable for the development of sub-aqueous avalanche or slumping; debris flows were recognized in the southern part of the basin (Sakai et al., 2002) but are restricted to the Pliocene stage of the paleo-lake (Sakai, 2001); e) gas expulsion during organic matter fermentation was not involved during deformation because no organic matter deposited in

the environment associated with soft-sediment deformation; f) the mean sedimentation rate of the lake was 0.1 mm/yr (Fujii et al., 2001) and such a slow sedimentation could not induce over-fluid pressure; g) other possible conditions for dike development, such as artesian conditions are not observed yet.

On the other hand, active Himalayan tectonics implies occurrence of earthquake shaking; hence geomorphologic and seismologic contexts are favorable for the development of seismites. Furthermore all the observed features have similar geometrical characteristics of structures linked to earthquake shaking, as defined by various workers (Beck, 2009; Gajurel, 2006; Heifetz et al., 2005 and Lignier, 2001; Moretti et al., 2002; Obermeier, 1996; Perucca and Moreiras, 2006; Rodriguez-Pascua et al., 2000; Rodriguez-Pascua et al., 2003; Tuttle and Sweig, 1996; Wheeler, 2002).

Therefore, we consider that the soft deformation and dike structures of the Plio–Pleistocene sediments of the Kathmandu basin are related to in-situ deformation of sediments during earthquake shaking, i.e. are seismites.

4.3. Characterization of paleo-intensity and seismites thickness

Some attempts (e.g. Sims, 1975) have been made to calibrate a relation between intensity and thickness of soft-sediment deformation levels. Rodriguez-Pascua et al. (2003) found that the frequency thickness distribution of 73 seismites obeys an exponential law, and that the "b" value of this distribution is the same as the "b" value for the Gutember and Richter law applied to the seismicity of the area. They deduced a linear function between thickness and intensity for small events producing soft-sediment deformation levels thinner than 7 cm. Hibsch et al. (1997) studied 20 seismites ranging from a few centimeters to 31 cm and suggested that thickness of soft-sediment deformation level is a power law function of the intensity for events greater than MMI V.

Comparison of previous studies clearly indicates a strong dispersion: the thickness of seismites linked to MMI VI events would vary between 12 cm for Hibsch et al. (1997)and 5 cm for Sims (1975). The dispersion is usually related to the influence of lithology, granulometry and sedimentary facies. For example, Moretti et al. (1999) have shown that the grain packing related to the pre-seismite sedimentary features is an important parameter for susceptibility to liquefaction. Nonetheless, other parameters may be hidden and a simplified physical approach is developed in the following to give some basis to analyze the controls of soft sediment thickness.

4.3.1. Horizontal acceleration and soil fluidization

Intensity of an earthquake is classically (e.g. Bolton and Idriss, 1982) considered as a logarithmic function of horizontal peak ground acceleration γ_h and numerous relationships have been proposed; for example Trifunac and Brady (1975) suggested that:

$$\log\gamma_{ah} = 0.014 + 0.30I_{mm} \quad (1)$$

where γ_{ah} is the average horizontal peak ground acceleration and I_{mm} is the MM Intensity.

We use a simplified approach of soil fluidization adapted from the geotechnical approach of Bolton and Idriss (1982) (Fig. 9A) to take into account the acceleration, the soil conditions and number of cycles of shaking in the thickness of the soft-sediment deformation.

In the soil, the shear stress τ is proportional to the acceleration γ and to the depth H (Bolton and Idriss, 1982):

$$\tau_{max} = \gamma^*_{max}(u_w/g)^* H^* P(H) \quad (2)$$

where u_w is the unit weights of the soil and g is the gravity acceleration. $P(H)$ is a function dependent of H that is not linear and always smaller than 1 (from Eq. (4), p. 76 of Bolton and Idriss, 1982).

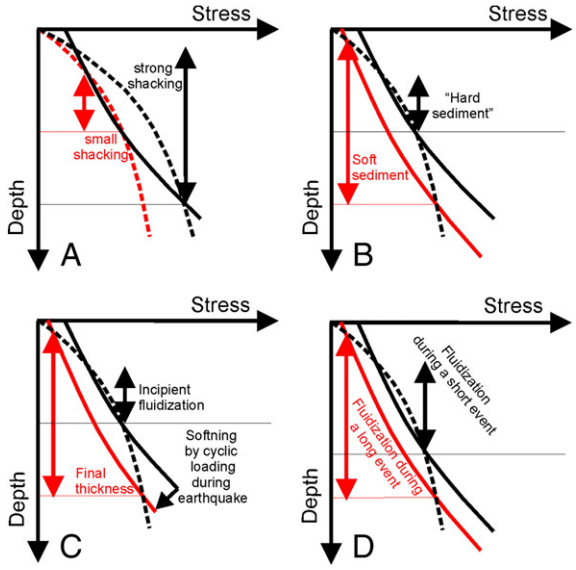

Fig. 9. Thickness of soft sediment deformation level inferred from shear strength versus depth evolution (adapted from Bolton and Idriss, 1982). Dashed line: shear stress level induced by an earthquake; thick lines: strength curve deduced from cyclic stress level causing fluidization; thin horizontal line: maximum depth where stress is stronger than strength; arrows: thickness of soft-sediment deformation layer. Comparison between strength curve and stress level induced by an earthquake is shown in sketches A to D: A) for the same lithology, a same type of seismic source, intensity of acceleration influences the final thickness: the far event induces smaller shaking, hence less stress and thinner soft-sediment deformation than a nearby event; B) the lithology (i.e. its shear strength) influences the final thickness: for a same shaking, a soft lithology would be affected by a thicker deformation than a harder lithology; C) a softening occurs when the number of cycles of stress loading increases. A thin incipient zone of fluidization forms at the beginning, then thickness of the soft sediment deformation increases due to softening of the sediment during cyclic loading; D) the number of shaking cycles influences the final thickness: for a same acceleration, a short shaking event related to less cyclic stress than a long shaking event induces a thinner soft sediment deformation level.

During cyclic loading of the upper part of the sediment (less than 10 m), Bolton and Idriss (1982) suggest that the average shear stress τ_{av} is:

$$\tau_{av} = \gamma^*_{ah}(u_w/g)^* H^*(0.65-0.004H). \quad (3)$$

This empirical relationship for the stress within the upper part of the sediment can be compared with experimental strength curves (Bolton and Idriss, 1982) that estimate the stress level causing liquefaction (thick lines on Fig. 9A, B, C and D refer to the bulk tendency found from these experiments). This comparison outlines that the horizontal acceleration is one of the major parameters that links seismite thickness and intensity. A qualitative comparison of the diagrams shows that: a) a greater acceleration (linked for example to the decrease of the distance between seismite locations and epicenter of earthquake) induces thickening of the soft-sediment deformation (Fig. 9A); b) the decrease of the strength induces an increase of the thickness; therefore "soft" sediment develops thicker deformation level than "hard" sediment (Fig. 9B).

4.3.2. Strain softening and seismites thickness

The strain softening (i.e. decreasing of the strength during the deformation) also influences the thickness: from experimental results, strength decreases gradually during the cyclic loading (Bolton and Idriss, 1982); when a critical threshold in the number of cycles is reached, fluidization begins and strong strain occurs. The strain softening is usually inferred for sand levels affected by a progressive increase of the fluid pressure, but silty levels could also develop strain softening (Bennet, 1989; Bolton and Idriss, 1982). A comparison of the

evolution of the stress threshold for liquefaction with the shear stress shows that: i) during a single event, the thickness of the soft-sediment deformation progressively increases due to the softening of the sediment during cyclic loading (Fig. 9C); ii) very close to the surface, a thin level could be preserved during the initial fluidization if the cohesion is not zero. Its deformation occurs when high deformation takes place beneath it; iii) thickness of a soft-sediment deformation is an increasing function of the number of shaking cycles during a seism (Fig. 9D).

Therefore a similar thickness could be theoretically obtained for two earthquakes either characterized by a great acceleration during few cycles or a smaller acceleration and a greater number of cycles. These two cases could respectively be related to a small magnitude earthquake occurring close to the seismite site and a great magnitude earthquake at a far distance. In this last case, the great acceleration at the source decreases with distance, but the small acceleration at the site is compensated by the long duration of the shaking.

4.3.3. Influence of vertical variation of the granulometry

The strength of sandy material increases faster with depth than the strength of silty material (e.g. Bolton and Idriss, 1982), and three effects of a granulometry contrast at the base of a silty material are evidenced: a) if a thin silty level stands above sandy levels, and if its thickness is smaller than the depth for which the shear stress becomes greater than the silt strength, no soft-sediment deformation develops (Fig. 10A); b) if the silty level is thicker than in the previous case but thinner than the depth for which the shear stress becomes again smaller than the silt strength, the thickness of the soft-sediment deformation is controlled by the granulometry contrast (Fig. 10B); c) if the silt level is thicker than the depth for which the shear stress becomes smaller than the silt strength, the thickness of the soft-sediment deformation is controlled by the acceleration (Fig. 10C).

4.3.4. Influence of vertical variation of the sedimentary facies

For the same granulometry, the physical properties could change due to the initial sedimentary features that peculiarly control the initial grain packing: during the cycles of shaking, the grain packing is reorganized, leading to a decrease of the porosity; if shaking affects water-saturated sediment and if a cap prevents fluid expulsion, an increase of the pore fluid pressure occurs and causes a major strain softening. This leads to soft-sediment deformation localized at depth beneath the impermeable cap (Fig. 10D). Such a process is enhanced for well-sorted sediment and for some specific sedimentary features like cross-laminated sands (Moretti et al., 1999).

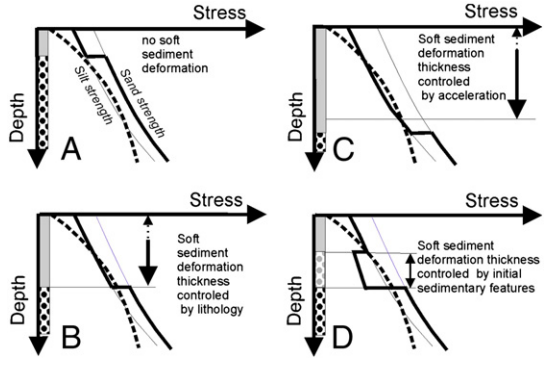

Fig. 10. Lithology contrast and thickness of soft-sediment deformation. The distribution of sandy and silty levels is shown on the vertical axis: gray for silty levels; black and gray dots for sandy level. A) If the silt that stands above sandier levels is very thin, the stress level is smaller than the cohesion and there is no soft-sediment deformation level. B) If the silty level is thinner than the depth inferred from the intersection of the shear stress and strength curves, all the silty level deforms and the thickness of the soft sediment deformation is controlled by the contrast of lithology. C) If the silty level is thicker than the depth of the intersection between the shear stress and silt strength curves, the thickness of the soft-sediment deformation is controlled by the acceleration. D) If a sand level is initially characterized by high porosity, grain re-organization during deformation increases the pore-fluid pressure and induces strain softening related to specific sedimentary features.

Another effect of vertical variation of granulometry and sedimentary facies would be related to reverse density gradient. The giant seismites (2–3 m thick) that occurred in a moderate seismicity area (Alfaro et al., 2010) are probably induced by gravity instabilities and they disappear laterally due to changes of sedimentary facies. We nonetheless consider that this gradient density effect is weak in the Kathmandu basin for the following reasons: a) the example developed in Section 3.5 confirms the role of horizontal shear, a result already found by Heifetz et al. (2005); b) we performed 3D densitometry studies of seismites with X-ray tomography technique (Colletta et al., 1991); this study was applied to 30 cm 30 cm 30 cm cubic samples and indicated a weak contrast of density, in the order of 10%, between sandy pillows and the surrounded silt.

4.3.5. Can we estimate paleo-intensity from seismites thickness?

Results of our simplified physical approach fit with numerous observations presented in Section 3:

- the granulometry control is clear in all the studied structures. Silty levels provide soft-sediment deformation close to the surface (Figs. 4, 6, 7, 8) and original sedimentary features with high porosity in sandy levels favor high fluid pressure and liquefaction beneath a cap; it is the case of the point bar sandy deposits at Godawari (Fig. 3) and at Gothatar (Fig. 7);
- the granulometry contrast between a soft silty upper part and a harder sandy lower part could limit the thickness of the deformation level; it is the case for the thin soft-sediment deformation example of Fig. 4 or the thicker one of Fig. 6;
- for slightly cohesive material, soft-sediment deformation does not exactly occur at the water/sediment interface but at few cm beneath the interface. Therefore, very thin silty levels could be preserved from deformation when deposited above sandy levels, a case exemplified by the thinning and lateral ending of the deformation of the silty level described in Section 3.4.2.
- thin sandy levels inter-bedded within a silty pile do not prevent the development of soft-sediment deformation structures and are passively deformed, like it is illustrated on Fig. 6.
- the deeper source level (unit a, Fig. 3A) for the last dike at Godawari (Section 3.3.1) fits with a deepening of the liquefaction level during a soleearthquake.

The physical approach that is developed predicts that:

- the thickness of the deformation level is mainly controlled by the acceleration only in the case of a very thick sediment pile dominated by silty component.
- the amount of deformation within a soft-sediment deformation feature decreases towards depth, due to the progressive increase of seismite thickness during a shacking event (Fig. 5B1). Nonetheless, thick soft-sediment deformation features can be related to a succession of shaking events if the sedimentation rate is smaller than the ratio thickness of a seismite divided by recurrence of seismic events; in this case, unconformities develop and deformation increases beneath the deformed unconformities (Fig. 5B2).
- a shaking event cannot only be described by one acceleration-linked parameter, and the duration and number of cycles also affect the final thickness of the deformation.

Therefore, the relationship between intensity and thickness of soft-sediment deformation is very complex and is not a bijection. Any "seismic scale" in the interpretation of seismites thickness has only a local significance due to site and lithological effects (Rodriguez-Pascua et al., 2000) and different intensity earthquakes could produce seismites of the same thickness.

In the following discussion, we mainly focus on the role of the contrast of granulometry and retain that thickness is an increasing function of intensity for a given lithology.

4.3.6. Comparison of historic and pre-historic seismites in the Kathmandu basin

The comparison of the seismites developed during the 1833 earthquake and the ~11 kyr BC event is possible because several conditions are similar during their development: a) the hydraulic conditions were similar for the seismites associated with the 26 August 1833 seism that formed during the monsoon season in the flooding plain of the Bagmati River and for the paleo-seismites that developed in the delta plain of the paleo-lake; b) the levels affected by soft-deformation have the same lithological characteristics at Koteswor, Gokarna and Gothatar sites, with soft-sediment deformation that mainly affects sandy silt; c) the Bagmati and Koteswor seismites are located in zones affected by the same amplification effect of the basin filling as suggested by the distribution of the 1934 damages (Fig. 2).

The Bagmati seismites have nearly a ~30 cm thickness not influenced by a lithological contrast (see Section 3.6.3). These seismites are located in an area where the village of Gokarna was more strongly affected by the 1833 earthquake than most of the Kathmandu valley villages (from Campbell, 1833, printed in Bilham, 1995). Therefore, though the gross estimation of the intensity in the Kathmandu basin varies from MM VIII to X (Bilham, 1995; Chitrakar and Pandey, 1986), the Gothatar and Gokarna sites have probably suffered an MM X intensity.

At Koteswor, the thickness of the ~11 kyr BC seismite is limited by the lithological contrast between the deformed silty level and the underneath undeformed sandy level. The maximum thickness of the seismite is 90 cm and gives a minimum value for the thickness of the soft-sediment deformation level induced by the ~11 kyr BP event. Because the Koteswor seismite is at least three times thicker than the Bagmati seismites, we consider that the intensity of the Koteswor earthquake was much greater than the intensity reached during the 1833 earthquake in the Gokarna area, i.e. greater than MMI X.

Fig. 11 shows the average shear stress level that would be reached at depth during the ~11 kyr BP and 1833 AD events. Only two constrains (thick horizontal lines on Fig. 11) allow to build the strength curve of the Kathmandu basin sediment and the width of the uncertainty domain outlines the difficulty to go farther in quantification.

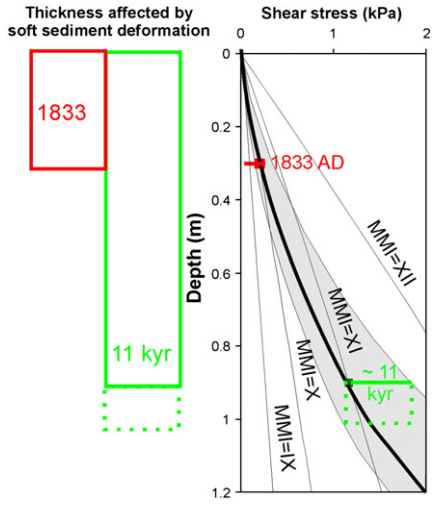

Fig. 11. A sketch of the stress level that affected the Kathmandu soft-sediment. Stress level curves for MM X, XI, XII Intensities deduced from a combination of Eqs. (1) and (3). The thick horizontal lines refer to the intensity of 1833 and ~11 kyr BC events and to the thickness of the associated soft-sediment deformation. The thick curve refers to a possible strength curve. Gray domain refers to the uncertainty concerning this curve.

4.4. Mega-earthquake occurrences in Himalaya

4.4.1. Paleo-seism record in the Kathmandu basin

The record of paleo-seisms is very discontinuous in fluvial sediment since ~10 kyr and numerous events, like the 1934 AD or 1255 AD earthquakes, are missing. Nonetheless, the ~11 kyr seismite indicates that earthquakes shocked the Kathmandu basin with an intensity greater than MMI X. Such intensity could not be related to earthquakes located at a shorter distance than the 1833 or 1934 events because their ruptures extended at a distance of less than 10 km from the center of Kathmandu (Bilham, 1995; Chen and Molnar, 1977). A minimum estimation of the ~11 kyr earthquake magnitude is obtained for a rupture that extended beneath the Kathmandu basin and even in this conservative case, the great seismite thickness is related to an event with a source magnitude greater than the 1934 event. The development of mega-seismites in the Kathmandu Valley during shaking events with magnitude greater than M 8.1 therefore argues for one interpretation among those proposed (Lavé et al., 2005) for the more than 14 m-surface slip that occurred during the ~1100 AD earthquake (trench 2 on Fig. 1): i) the 14 m-surface slip could be the sum of several surface motions occurring during a short period and therefore difficult to individualize from trench dating; ii) it could be related to an earthquake that released the elastically stored deformation at the tip of previous ruptures restricted to the northern part of Himalaya; the ~1100 AD earthquake would finally deliver to the surface a sum of several events; ii) medieval-like earthquakes could nucleate below the High Himalaya, and break through the surface trace of the MFT, leading to cross-strike distance along the MHT of about 100 km. We favor this last seismo-tectonic interpretation that agrees with great seismite thickness and large surface displacement, hence $M \geq 8.6$ paleo-earthquakes (Lavé et al., 2005).

4.4.2. The 1255 AD event

The 1255 AD event badly damaged Kathmandu and is the most catastrophic event recorded in the Nepalese historic archives (e.g. Shava, 1992). Localization of its epicenter from historical archives is not possible because information is restricted to the Kathmandu area. In order to precise the location of the 1255 event, a cross-section through the MFT is described in the following and several ^{14}C ages (Table 3) are added to a previous study performed in the western Nepal (Mugnier et al., 2005).

In the western Nepal, (site 3 on Fig. 1), the MFT thrusts above 1225–1271 yr Cal AD sediment (Table 3 and Mugnier et al., 2005) and a terrace (T5) is folded above the MFT (Fig. 12D) with ~6 m vertical offset. Six hundred meters north of the MFT, T5 is located ~13 m above the present-day river bed and ~9 m above the T2 terrace (Fig. 12C). The T5 definitive abandonment occurred after 1398–1442 Cal AD from a charcoal sample (Table 3). As the abandonment occurred after the uplift related to the earthquake, the uplift occurred between 1225 and 1442 Cal AD. We thus suggest that ~8 m slip occurred along the MFT in relation with the 1255 AD seismic event and caused ~6 m uplift of the hanging-wall; the knick point retreat that controls the upstream incision (Whipple, 2004) would occurred at a rate of 3–4 m/yr in order to induce the abandonment of the upstream part of T5 terrace between 1398 and 1442 Cal AD. An alternative interpretation is that the 8 m-surface-slip is the sum of several events and would explain the abandonment of several small terrace levels (T3 and T4) (Mugnier et al., 2005). However, complementary studies indicate that T3 was ascribed to a debris flow of 5 m thick and T4 is of very small extension. The post 1832–1885 Cal AD incision of terrace T2 that seals the MFT could either be related to entropic influence or to uplift above a blind tip of the MHT; two great earthquakes of MMI VIII were quoted in this area for the 19th century (Khattri, 1987; Quitmeyer and Jacob, 1979) and also shocked Kathmandu (Chitrakar and Pandey, 1986); we favor the 1866 AD event rather than the 1833 AD event that occurred eastward (see Section 2.2).

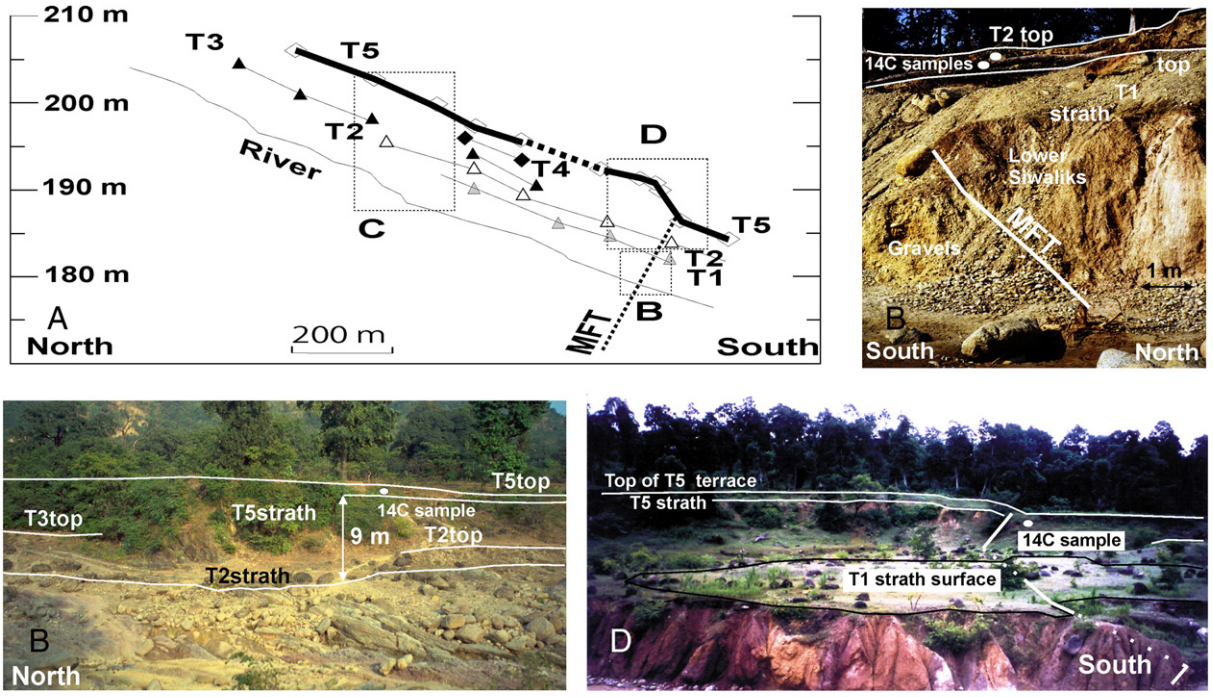

Fig. 12. The 1255 surface rupture of the MFT (western Nepal, site 3 on Fig. 1). A) Profiles of river and of T1 to T5 terraces at Koilabas. Rectangles refer to Fig. 11B, C and D; B). Conglomerate at the footwall of the MFT; recent strath surfaces (T1 and T2) indicate incision of hanging- and foot-walls of the MFT dated from ^{14}C samples (00–15 and 00–16 in T2) at 1832–1885 Cal AD; T1 is a modern terrace and contains plastic bags; C) Uplifted strath terrace T5, 600 m to the north of the MFT. The last flooding event above this terrace is dated at 1398–1442 yr Cal AD (^{14}C sample 00–09); D) A view of the scarp at the hanging-wall of the MFT, that formed after 1225–1271 yr Cal AD (from ^{14}C sample 00–20).

The location of the MFT at the Nepal/India border has nonetheless prevented any trenching through the MFT trace for administrative reasons, preventing more definitive conclusion.

In summary, we believe that, even in the case of successive events, the 1255 AD event delivers slip to the surface in the western Nepal.

4.4.3. Evidence for successive medieval mega-earthquakes

The ~1100 Cal AD rupture evidenced by trenching in eastern Nepal (Nakata et al., 1998) cannot be linked to the 1255 AD historic destruction of Kathmandu: 4 dated organic samples deposited after the earthquake indicate a rupture prior to 1160 Cal AD (with a probability of 95%, Lavé et al., 2005). The 1255 earthquake is also distinct from the rupture which transferred ~18 m-slip to the surface in Kumaon and far western Nepal during the ~15th century (Kumar et al., 2006, 2010; Yule et al., 2007): one ^{14}C sample in the western trench of Kumaon (6 on Fig. 1) indicates an occurrence after 1282 Cal AD (with a probability of 95%) and 2 samples in the trench located eastward (5 on Fig. 1) respectively indicate an occurrence after 1278 Cal AD and 1259 Cal AD (with a probability of 95%); the compilation of the whole ^{14}C dating suggests an interval between 1282 and 1433 Cal AD (Kumar et al., 2006) and we suggest that this mega-earthquake affected Kathmandu in 1408 AD with a MMI X (Chitrakar and Pandey, 1986).

Therefore three mega-earthquakes affected Kathmandu during the 12th, 13th and 15th centuries: an event of magnitude greater than M 8.6 occurred in ~1100 Cal AD in the eastern Nepal; an event, that occurred in the western Nepal, dead 1/3 of the population in 1255 AD and an event of magnitude greater than M 8.6 occurred in 1408 AD in the far western Nepal.

4.4.4. Mega-earthquakes and along-Himalayan-arc asperities

The seismic cycle in the Himalaya is presumably due to a growth of the ruptures impeded by the presence of along-arc asperities (Feldl and Bilham, 2006). Every rupture does not necessarily release all

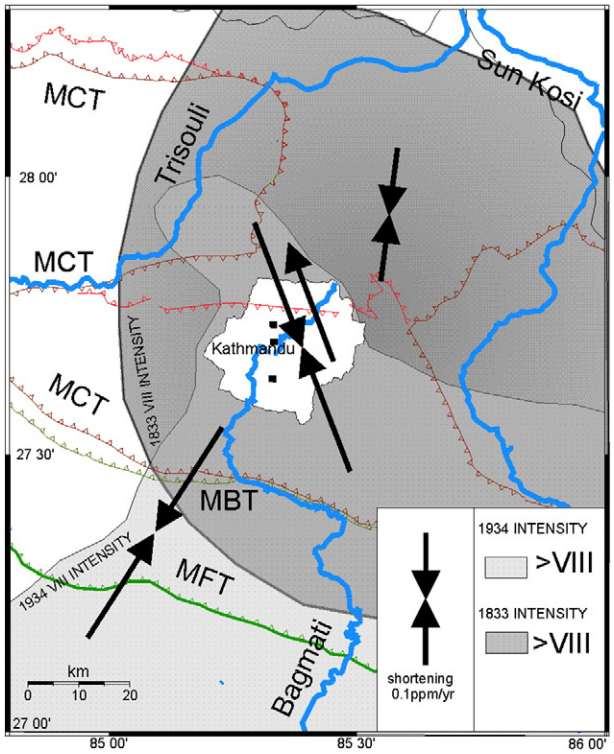

Fig. 13. A structural map of the Himalayan belt at the longitude of Kathmandu. Distribution of VIII Intensity adapted from Pandey and Molnar (1988) for 1934 earthquake (MMI) and from Ambraseys and Douglas (2004) for 1833 earthquake (MSK). Present-day shortening from Jouanne et al. (2004).

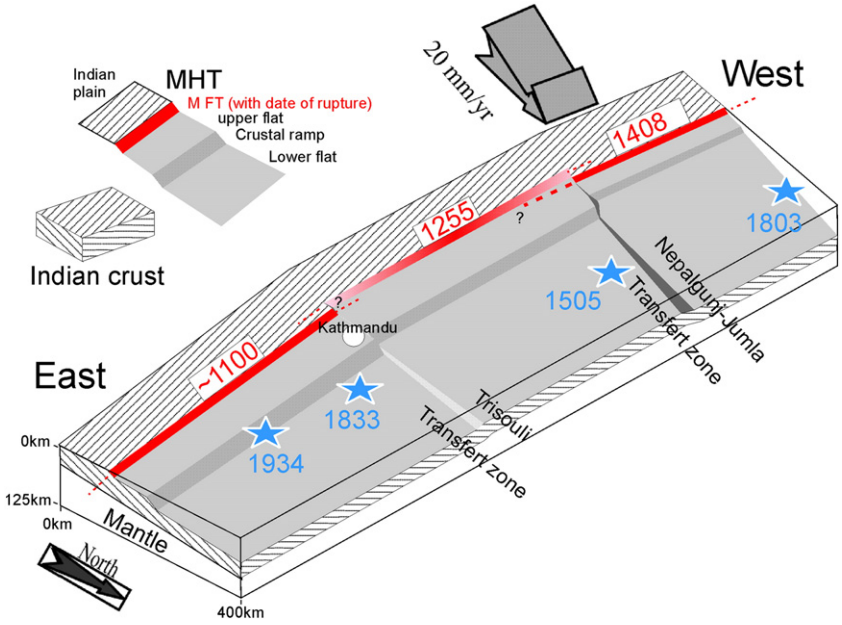

Fig. 14. A sketch of the geometry of the MHT at crustal scale (adapted from Berger et al., 2004) with epicenter of the great historical earthquakes (blue stars) and frontal rupture (red lines) adapted from Kumar et al., 2010 and this paper. "Nepalgunj-Jumla Transfer Zone" and "Trisouli Transfer Zone" are crustal lateral ramps inferred from mechanic modeling (Berger et al., 2004), thermal modeling (Robert et al., 2011) and cartographic pattern of the structures (Mugnier et al., 1999 and this paper).

displacement stored elastically by the southern Tibet and the great earthquake slip is mainly related to the length between along-arc asperities (Feldl and Bilham, 2006).

We suggest that an along-arc asperity is located close to Kathmandu. This asperity is related to one of the transfer zones along the MHT (Fig. 14) inferred by Berger et al. (2004) and Robert et al. (2011). This transfer zone would be located beneath the Trisuli River and induces: a) a greater uplift of the Lesser Himalayan rocks in its western side that causes the dramatic cartographic bend of the MCT in this area (Fig. 13); b) a singularity in respect to the usual N 10°E to N 20°E shortening direction that is here deviated towards the N 150°E direction (Jouanne et al., 2004; Fig. 13); c) a north–south boundary for the zones of MMI>VIII during the 1833 and 1934 events. At the scale of the Central Himalaya, the distribution of great earthquakes outlines the role of another transfer zone: the "Jumla-Nepalgunj Transfer Zone" (Mugnier et al., 1999): between the two transfer zones, the 1255 great earthquake occurred and caused the destruction of Kathmandu and this area is a seismic gap since 1505 (Ambraseys and Jackson, 2003) or could be affected in 1866 AD by an event (see Section 4.4.2); to the west of this transfer zone, numerous medium scale instrumental earthquakes are recorded and a mega-thrust occurred in 1410 (see discussion in Section 4.2.3).

Table 4
Paleoseisms and historic earthquakes in the Kathmandu area (Intensity MMI greater than VII in Kathmandu).

Date	Source of information	Intensity (MMI)	Magnitude (Mw)	Epicenter or general localization	Main reference
Cal–11 kyr BC	Seismite	≥XI		?	This paper
Cal–1100 AD	Trench	≥X[a]	~8.5	Surface rupture eastern Nepal	Lavé et al. (2005)
1255 AD (6/7)	Historic (only KTM) and Trench	X		Surface rupture western Nepal[i]	Chitrakar and Pandey (1986) This paper
1408 AD	Historic (only KTM) and Trench	X	>8.5[b]	Surface rupture in far western Himalaya[b]	Chitrakar and Pandey (1986)
1505 AD	Historic (Only regional, not in KTM)	≥VII[c]	8.16[d]	N34.50°, E 69.10°	Ambraseys and Jackson (2003)
1681 AD	Historic	IX			Chitrakar and Pandey (1986)
1767 AD	Historic	≥VII			NSET (2006)
1810 AD	Historic	IX		Eastern Nepal?[e]	Chitrakar and Pandey (1986)
1833 AD (8/26)	Historic	IX–X	7.61[f]	N28.00°, E86.00°[f]	Bilham (1995)
1833 AD (10/04)	Historic	IX	~7?	Central Nepal (South of KTM)?[g]	Chitrakar and Pandey (1986)
1833 AD (10/18)	Historic	VIII	~7?	Central Nepal (South-West of KTM)?[g]	Chitrakar and Pandey (1986)
1866 AD (5/23)	Historic (regional and KTM)	VIII	7.6?[h]	Central[h] or western[i] Nepal	Oldham (1883) in Khattri (1987)
1934 AD (1/15)	Instrumental and historic	X	8.11[d]	N27.55°, E 87.09°	Chen and Molnar (1977) Pandey and Molnar (1988)

[a] From the magnitude estimation of Lavé et al. (2005) and a comparison with the Intensity of the 1934 event.
[b] From a compilation of trenching indicating a ~1410 AD rupture in western Himalaya (Kumar et al., 2010).
[c] Estimated in this study from Eq. (2) of Ambraseys and Douglas (2004).
[d] From Ambraseys and Douglas (2004).
[e] From Chandra (1992), this event was strongly felt in Calcutta (MMI=V).
[f] Estimated by Thapa (1997).
[g] From Chandra (1992) and Bilham (1995): strong aftershocks were felt simultaneously on the 4 October 1833 at Kathmandu, Allahabad, Berhampore, Malda, Purneah, Monghyr and Bhagalpore, and on the 18 October at Goruckpur, Kathmandu and Allahabad.
[h] From Khattri (1987).
[i] This study.

5. Conclusions

This study clearly illustrates that soft-sediment deformation in the Kathmandu basin is mainly controlled by the fluidization of silty levels during earthquake shaking. We link the soft-sediment deformation features to earthquakes because of their synchronicity with historic seismic events or dike initiation. Structural studies suggest that waves inducing shearing between planes parallel to the surface are a major cause for soft-sediment deformation; the fluidization of the silty levels during earthquake shaking completely de-organizes the initial tabular attitude of the sediment close to the sediment/water interface, and the sandy levels inter-bedded in the silty deposits are rather passively deformed. Although the thickness of the soft-sediment deformation increases with the intensity of the shaking, we demonstrate that there is not a univocal relationship between thickness and MM Intensity: lithology and duration of the shaking must also be taken into account.

A pre-historic soft-sediment deformation level is three times thicker than those developed in the same lithology during historic events of MMI X. We therefore suggest that this soft-sediment deformation level is related to an earthquake the magnitude of which was greater than the historical M~8.1 events. This new result supports the previous interpretation that the large surface displacements evidenced by trenching were linked to mega-earthquakes with magnitude much greater than the historical M~8.1 earthquakes and agree with a seismo-tectonic model where mega-earthquakes (greater than ~8.6) could occur in Himalaya.

Concerning the seismic hazard in the Kathmandu basin, a calendar of the earthquakes with an Intensity (MM) greater than VII is proposed (Table 4) and upgrades the previous one. The study of the seismites in the Kathmandu basin indicates the occurrence of events more intense than the well known 20th and 19th century ones. Furthermore structural framework and paleo-seismologic studies suggest that Kathmandu is at the transition between 2 seismo-tectonic segments of Himalaya and could be badly affected by earthquakes respectively located at the east and at the west of the city. Due to this peculiar location, successive mega-earthquakes could affect the city in a short time interval. This catastrophic succession probably occurred in the 12th and 13th centuries. Such worst scenario has to be kept in mind for the planning of the post-earthquake management: the occurrence of a catastrophic earthquake would not mean that Kathmandu would then be safe for a long period at the human scale.

Acknowledgments

The work was funded by the French program ANR (Paksis). A. Gajurel benefited from a Grenoble University grant during a three month stay in Grenoble. We thank J. Perumal, M. Moretti, C. Beck and L. Audin for numerous discussions. The comments of F. Storti and three anonymous reviewers help to clarify the text.

References

Alfaro, P., Guibert, L., Moretti, M., Garcia-Tortosa, J., Sanz de Galdenao, C., Galindo-zaldivar, J., Lopez-Garrido, C., 2010. The significance of giant seismites in the Plio–Pleistocene baza paleo-lake (S. Spain). Terra Nova 22, 172–179.

Ambraseys, N.N., Jackson, D., 2003. A note on early earthquakes in northern India and southern Tibet. Curr. Sci. 84, 571–582.

Ambraseys, N.N., Douglas, J., 2004. Magnitude calibration of north Indian earthquakes. Geophys. J. Int. 158, 1–42.

Avouac, J.P., 2003. In: Dmowska, R. (Ed.), Mountain building, erosion and the seismic cycle in the Nepal Himalaya. Advances in Geophysics, vol. 46. Elsevier, Amsterdam, pp. 1–80. doi:10.1016/S0065-2687(03)46001-9.

Banerjee, P., Burgmann, R., 2002. Convergence across the northwest Himalaya from GPS measurements. Geophys. Res. Lett. 29 (13), 1652. doi:10.1029/2002GL015184.

Beck, C., 2009. Lake sediments as Late Quaternary palaeo-seismic archives: examples in north-western Alps and clues for earthquake-origin assessment of sedimentary disturbances. Earth Sci. Rev. 96, 327–344.

Bennet, M.J., 1989. Liquefaction analysis of the 1971 ground failure at the San Fernando Juvenil Hall. Bull. Assoc. Eng. Geol. 26, 209–226.

Berger, A., Jouanne, F., Hassani, R., Mugnier, J.L., 2004. Modelling the spatial distribution of present-day deformation in Nepal: how cylindrical is the Main Himalayan Thrust in Nepal? Geophys. J. Int. 156, 94–112.

Bettinelli, P., Avouac, J.P., Flouzat, M., Jouanne, F., Bollinger, L., Willis, P., Chitrakar, G.R., 2006. Plate motion of India and interseismic strain in the Nepal Himalaya from GPS and DORIS measurements. J. Geodesy 80, 567–589.

Bilham, R., 1995. Location and magnitude of the 1833 Nepal earthquake and its relation to the rupture zones of contiguous great Himalayan earthquakes. Curr. Sci. 69, 101–127.

Bilham, R., Larson, K., Freymuller, J., Project IDYLIM members, 1997. Indo-Asian collision rates in the Nepal. Nature 386, 61–64.

Bilham, R., Gaur, V.K., Molnar, P., 2001. Himalayan seismic hazard. Science 293, 1442–1444.

Bolton, H., Idriss, I., 1982. Published by the Ground motion and soil liquefaction during earthquake. Earthquake Engineering Research Institute. 134 pp.

Campbell, A., 1833. Further particulars of the Earthquake in Nepal. J. Asiatic Soc. Bengal 2, Misc. VI, 636–639.

Chandra, U., 1992. Seismotectonics of Himalaya. Curr. Sci. 62, 40–72.

Chen, W., Molnar, P., 1977. Seismic moments of major earthquakes and the average rate of slip in central Asia. J. Geophys. Res. 82, 2945–2969.

Chitrakar, G.R., Pandey, M.R., 1986. Historical earthquakes of Nepal. J. Nepal Geol. Soc. 4, 7–8 1986.

Colletta, B., Letouzey, J., Pinedo, R., Ballard, J.F., Bale, P., 1991. Computerized X-ray tomography analysis of sandbox models: examples of thin skinned systems. Geology 19, 1063–1067.

Cotton, F., Campillo, M., Deschamps, A., Rastogi, B., 1996. Rupture history and seismotectonics of the 1991 Uttarkashi, Himalayas earthquake. Tectonophysics 258, 35–51.

De Celles, P.G., Gehrels, G.E., Quade, J., Ojha, T.P., Kapp, P.A., 1998. Neogene foreland basin deposits, erosional unroofing and the kinematic history of the Himalayan fold-thrust belt, Western Nepal. Geol. Soc. Am. Bull. 110, 2–21.

Dixit, A., Dwelly-Samant, L., Nakarmi, M., Tucker, B., Pradhanang, S., 1998. The Kathmandu valley Earthquake management plan. Published by National Society for Earthquake Technology-Nepal37 pp. www.preventionweb.net/english/professional/publications/v.php?id=1496.

Dunn, J., Auden, J., Gosh, A., Roy, S., 1939. published by The Bihar–Nepal earthquake of 1934. Mem. Geol. Soc. of India, vol. 73. Survey of India, Calcutta. 391 pp.

Feldl, N., Bilham, R., 2006. Great Himalayan earthquakes and the Tibetan plateau. Nature 444, 165–170.

Fujii, R., Kuwahara, Y., Sakai, H., 2001. Mineral composition changes recorded in the sediments from a 284-m-long drill-well in the central part of the Kathmandu Basin, Nepal. J. Nepal Geol. Soc. 25, 63–69.

Gajurel, A.P., Huyghe, P., France-Lanord, C., Mugnier, J.L., Upreti, B.N., Le Fort, P., 1998. Seismites in the Kathmandu basin Nepal. J. Nepal Geol. Soc. 18, 125–134.

Gajurel, A.P., Huyghe, P., Upreti, B.N., Mugnier, J.L., 2000. Palaeoeismicity in the Koteswor area of the Kathmandu Valley, Nepal, inferred from the soft-sediment deformational structures. J. Nepal Geol. Soc. 22, 547–556.

Gajurel, A., Huyghe, P., Sukhija, B., Mugnier, J.L., Reddy, D., Upreti, B., 2002. Paleoseismological investigations in the Kathmandu Valley, Nepal: soft sediment deformation and liquefaction structures. Symposium on Seismology, Earthquake Hazard Assessment and Risk management, Kathmandu, 24–26 November 2002, pp. 132–133.

Gajurel, A., 2006. Etude sédimentologique et géochimique (isotopes stables) des basins syn-orogéniques de l'Himalaya du Népal (Siwaliks et basin de Kathmandu). PhD thesis Grenoble University, 301 pp.

Gautam, P., Hosoi, A., Sakai, T., Arita, K., 2001. Magnetostratigraphic evidence for the occurrence of pre-Brunhes (>780 kyr) sediments in the northwestern part of the Kathmandu Valley Nepal. J. Nepal Geol. Soc. 25 (sp. Issue), 99–109.

Gayer, E., Lavé, J., Pik, R., France-Lanord, C., 2006. Monsoonal forcing of Holocene glacier fluctuations in Ganesh Himal (Central Nepal) constrained by cosmogenic 3He exposure ages of garnets. Earth Planet. Sci. Lett. 252, 275–288.

Heifetz, E., Agnon, A., Marco, S., 2005. Soft sediment deformation by Kelvin Helmholtz Instability: a case from Dead Sea earthquakes. Earth and Planetary Sci. Lett. 236, 497–504.

Hibsch, C., Alvarado, A., Yepes, H., Perez, V.H., Sébrier, M., 1997. Holocene liquefaction and soft-sediment deformation in Quito (Ecuador): a paleoseismic history recorded in lacustrine. J. Geodyn. 24, 259–280.

Jouanne, F., Mugnier, J.L., Gamond, J.F., Le Fort, P., Pandey, M.R., Bollinger, L., Flouzat, M., Avouac, J.P., 2004. Current shortening across the Himalaya of Nepal. Geophys. J. Int. 157, 1–14.

Kaneda, H., Nakata, T., Tsutsumi, H., Kondo, H., Sugito, N., Awata, Y., Akhtar, S.S., Majid, A., Khattak, W., Awan, A.A., Yeats, R.S., Hussain, A., Ashraf, M., Wesnousky, S.G., Kausar, A.B., 2008. Surface Rupture of the 2005 Kashmir, Pakistan, earthquake and its active tectonic implications. Bull. Seismol. Soc. Am. 98, 521–557. doi:10.1785/0120070073.

Katel, T.P., Upreti, B.N., Pokharel, G.S., 1996. Engineering properties of fine grained soils of Kathmandu valley, Nepal. J. Nepal Geol. Soc. 14, 121–138.

Khattri, K., 1987. Great earthquakes, seismicity gaps and potential for earthquake disaster along the Himalaya plate boundary. Tectonophysics 138, 79–92.

Kumar, S., Wesnousky, S., Rockwell, T.K., Briggs, R.W., Thakur, V.C., Jayangondaperumal, R., 2006. Paleoseismic evidence of great surface rupture earthquakes along the Indian Himalaya. J. of Geophysical Res. 111, B03304. doi:10.1029/2004JB003309.

Kumar, S., Wesnousky, S., Jayangondaperumal, R., Nakata, T., Kumahara, Y., Singh, V., 2010. Paleoseismological evidence of surface faulting along the northeastern

Himalayan front, India: Timing, size, and spatial extent of great earthquakes. J. Geophys. Res. 115, B12422, 20 pp., 2010. doi:10.1029/2009JB006789.
Larson, E., 1999. Global centroid moment tensor catalog. http://www.globalcmt.org/CMTsearch.html.
Lavé, J., Avouac, J.P., 2001. Fluvial incision and tectonic uplift across the Himalayas of Central Nepal. J. Geophys. Res. 106, 26561–26592.
Lavé, J., Yule, D., Sapkota, S., Bassant, K., Madden, C., Attal, M., Pandey, R., 2005. Evidence for a great Medieval earthquake (1100 AD) in the central Himalayas, Nepal. Science 307, 1302–1305.
Le Fort, P., 1975. Himalayas: the collided range. Present knowledge of the continental arc. Am. J. Sci. 275, 1–44.
Levi, T., Weinberger, R., Aïfa, T., Eyal, Y., Marco, S., 2006. Injection mechanism of clay-rich sediments into dikes during earthquakes. Geochem. Geophys. Geosysts. 7 (Q12009). doi:10.1029/2006GC001410.
Lignier, V., 2001. Les sédiments lacustres et l'enregistrement de la paléosismicité. PhD University of Savoie, 230 pp.
Malkawi, A.I.H., Alawneh, A.S., 2000. Paleoearthquake features as indicators of potential earthquake activities in the Karameh DamSite. Nat. Hazards 22, 1–16.
Menzies, J., 2002. Modern and Past Glacial Environments. In: Butterworth, Heinemann (Ed.), p. 576. ISBN 10: 0-7506-4226-2.
Molnar, P., 1987. The distribution of intensity associated with the 1905 Kangra earthquake and bounds on the extent of the rupture zone. J. Geol. Soc. India 29, 221–229.
Molnar, P., 1990. A review of the seismicity and the rates of active underthrusting and deformation at the Himalaya. J. Himalayan Geol. 1, 131–154.
Moretti, M., Alfaro, P., Caselles, O., Canas, J.A., 1999. Modelling seismites with a digital shaking table. Tectonophysics 304, 369–383.
Moretti, M., Pieri, P., Tropeano, M., 2002. Late Pleistocene soft-sediment deformation structures interpreted as seismites in paralic deposits in the City of Bari (Apulian foreland — Southern Italy). Geol. Soc. Am. Spec. Pap. 359, 75–85.
Moretti, M., Sabato, L., 2007. Recognition of trigger mechanisms for soft-sediment deformation in the Pleistocene lacustrine deposits of the Sant'Arcangelo Basin (Southern Italy): seismic shock vs. overloading. Sediment. Geol. 196, 31–45.
Moribayashi, S., Maruo, Y., 1980. Basement topography of the Kathmandu valley Nepal: an application of gravitational method to the survey of a tectonic basin in Himalayas. J. Jap. Soc. Eng. Geol. 21, 30–37.
Mugnier, J.L., Leturmy, P., Mascle, G., Huyghe, P., Chalaron, E., Vidal, G., Husson, L., Delcaillau, B., 1999. The Siwaliks of western Nepal: I — geometry and kinematics. J. Asian Earth Sci. 17, 629–642.
Mugnier, J.L., Huyghe, P., Leturmy, P., Jouanne, F., 2004. Episodicity and rates of thrust sheet motion in Himalaya (Western Nepal). In: Mc, Clay (Ed.), Thrust Tectonics and Hydrocarbon System: American Association of Petroleum Geologists Memory, 82, pp. 91–114.
Mugnier, J.L., Huyghe, P., Gajurel, A.P., Becel, D., 2005. Frontal and piggy-back seismic ruptures in the external thrust belt of western Nepal. J. Asian Earth Sci. 25, 707–717.
Nakata, T., Kumura, K., Rockwell, T., 1998. First successful paleoseismic trench study on active faults in the Himalayas. Proceedings of AGU 1998 Fall Meeting: Eos, Transactions AGU, 79, p. 45.
NSET, 2006. Recorder History of Earthquakes in Nepal: Past Earthquakes in Nepal. http://www.nset.org.np/nset_new/html/Earthquake_History.html.
Obermeier, S., 1996. Using liquefaction-induced features for paleoseismic analysis. In: paleoseismology, edited by McCalpin. J. Int. Geophysics Ser. 62, 331–396.
Obermeier, S., Pond, E., Olson, S., Green, R., 2002. Paleoliquefaction studies in continental settings. Geol. Soc. Am. Spec. Pap. 359, 13–27.
Oldham, T., 1883. A catalogue of Indian earthquakes from the earliest time to the end of A.D. 1869. Mem. Geol. Surv. India 19, 163–215.
Oldham, R., 1917. The structures of Himalaya and of the Gangetic plain, as elucidated by geodetic observations in India. Mem. Geol. Surv. India 42, 149–301.
Owen, G., Moretti, M., 2008. Determining the origin of soft-sediment deformation structures: a case study from Upper Carboniferous delta deposits in south-west Wales, UK. Terra Nova 20, 237–245. doi:10.1111/j.1365-3121.2008.00807.x.
Pandey, M.R., Molnar, P., 1988. The distribution of intensity of the Bihar-Nepal earthquake of 15 January 1934 and bounds on the extent of the rupture zone. J. Geol. Soc. Nepal 5, 22–44.
Pandey, M.R., Tandukar, R.P., Avouac, J.P., Lavé, J., Massot, J.P., 1995. Evidence for recent interseismic strain accumulation on a mid-crustal ramp in the Central Himalaya of Nepal. Geophys. Res. Lett. 22, 751–758.
Pandey, M.R., Tandukar, R.P., Avouac, J.P., Vergne, J., Héritier, Th., 1999. Characteristics of seismicity of Nepal and their seismotectonic implications. J. Asian Earth Sci. 17, 703–712.
Perucca, L., Moreiras, S., 2006. Liquefaction phenomena associated with historical earthquakes in San Juan and Mendoza Provinces, Argentina. Quatern. Int. 158, 96–109.
Paudayal, K.N., Ferguson, D.K., 2004. Pleistocene palynology of Nepal. Quat. Int. 117, 69–79.
Quitmeyer, R.C., Jacob, K.H., 1979. Historical and modern seismicity of Pakistan, Afghanistan, Northwestern India, and Southeastern Iran. Bull. Seismol. Soc. Am. 69, 773–823.
Rai, S., 2001. Geology, geochemistry, and radiochronology of the Kathmandu and Gosainkund crystalline nappes, central Nepal Himalaya. J. Nepal Geol. Soc. 25, 135–155.
Rana, B.J.B., 1935. Nepal Ko Maha Bhukampa. Jorganesh press.
Rana, G., Murray, B., Maharjan, D., Thaku, A., 2007. Kathmandu Valley Environment Outlook. http://www.rrcap.unep.org/reports/eo/kv/KVEO_0_cover.pdf. published by ICIMOD, Kathmandu, 118 pp.
Rastogi, B., Chadha, R., 1995. Intensity and isoseismals of Uttarkashi earthquake of October, 1991. In: Gupta, H.K., Gupta, G.D. (Eds.), Uttarkashi Earthquake: Geological Society of India, Memoir, 30, pp. 19–24.
Reimer, P.J., Baillie, M.G.L., Bard, E., Bayliss, A., Beck, J.W., Bertrand, C.J.H., Blackwell, P.G., Buck, C.E., Burr, G.S., Cutler, K.B., Damon, P.E., Edwards, R.L., Fairbanks, R.G., Friedrich, M., Guilderson, T.P., Hogg, A.G., Hughen, K.A., Kromer, B., McCormac, G., Manning, S., Ramsey, C., Reimer, R.W., Remmele, S., Southon, J.R., Stuiver, M., Talamo, S., Taylor, F.W., Van der Plicht, J., Weyhenmeyer, C.E., 2004. IntCal04 terrestrial radiocarbon age calibration, 0–26 cal kyr BP. Radiocarbon 46, 1029–1058.
Robert, X., van der Beek, P.A., Braun, J., Perry, C.M., Mugnier, J.-L., 2011. Control of detachment geometry on lateral variations in exhumation rates in the Himalaya: Insights from low-temperature thermochronology and numerical modeling. J. Geophys. Res. 116, B05202, 22 pp., doi:10.1029/2010JB007893.
Rodriguez-Pascua, M., DeVicente, G., Calvo, J.P., Gomez-Gras, D., 2000. Soft-sediment deformation structures interpreted as seismites in lacustrine sediments of the Prebetic Zone, SE Spain, and their potential use as indicators of earthquake magnitudes during the late Miocene. Sediment. Geol. 135, 117–135.
Rodriguez-Pascua, M., Calvo, J.P., DeVicente, G., Gomez-Gras, D., 2003. Similarities between recent seismic activity and paleoseismites during the late miocene in the external Betic Chain (Spain): relationship by "b" value and the fractal dimension. J. Struct. Geol. 25, 749–763.
Sakai, H., 2001. Stratigraphic division and sedimentary facies of the Kathmandu Basin Group, Central Nepal. J. Nepal Geol. Soc. 25 (sp. Issue), 19–32.
Sakai, T., Gajurel, A.P., Tabata, H., Upreti, B.N., 2001. Small-amplitude lake-level fluctuations recorded in aggrading deltaic deposits of the Upper Pleistocene Thimi and Gokarna formations, Kathmandu Valley. J. Nepal Geol. Soc. 25 (sp. Issue), 43–51.
Sakai, H., Fujii, R., Kunwahara, Y., 2002. Changes in the depositional system of the Paleo-Kathmandu Lake caused by uplift of the Nepal Lesser Himalayas. J. Asian Earth Sci. 20, 267–276.
Sakai, T., Takagawa, T., Gajurel, A.P., Tabata, H., O'I, N., Upreti, B.N., 2006. Discovery of sediment indicating rapid lake-level fall in the late Pleistocene Gokarna Formation, Kathmandu Valley, Nepal: implication for terrace formation. Quatern. Res. 45, 99–112.
Schelling, D., Arita, K., 1991. Thrust tectonics, crustal shortening, and the structure of the far-eastern Nepal Himalaya. Tectonics 10, 851–862.
Schulte-Pelkum, V., Monsalve, G., Sheehan, A., Pandey, M.R., Sapkota, S., Bilham, R., Wu, F., 2005. Imaging the Indian subcontinent beneath the Himalaya. Nature 435, 1222–1225.
Seeber, L., Armbruster, J., 1981. Great detachment earthquakes along the Himalayan arc and long term forecast. In: Sibson, D.W., Richards, P.G. (Eds.), Earthquake Prediction: An International Review. Maurice Ewing Series, 4. Amererican Geophysical Union, Washington D.C, pp. 259–277.
Seilacher, A., 1991. Events and their signatures — an overview. In: Einsele, G., Ricken, W., Seilacher, A. (Eds.), Cycles and Events in Stratigraphy. Springer-Verlag, Berlin Heidelberg, pp. 222–226.
Shava, R., 1992. Ancient and Medieval Nepal. Manohar Publication, New-Delhi. 155 p.
Sims, J.D., 1975. Determinating earthquake recurrence intervals from deformational structures in young lacustrine sediments. Tectonophysics 29, 141–152.
Stuiver, M., Reimer, P.J., Bard, E., Beck, J.W., Burr, G.S., Hughen, K.A., Kromer, B., McCormac, F.G., v. d. Plicht, J., Spurk, M., 1998. INTCAL98 Radiocarbon age calibration 24,000–0 cal BP. Radiocarbon 40, 1041–1083.
Srivastava, P., Mitra, G., 1994. Thrust geometries and deep structure of the outer and lesser Himalayas, Kumaon of the Himalayan fold-and-thrust belt. Tectonics 13, 89–109.
Thapa, G.S., 1997. Microseismic epicenter map of Nepal Himalaya and adjoining region. Edited by Department of Mines and Geology, Kathmandu, Nepal.
Trifunac, M., Brady, A., 1975. On the correlation of seismic intensity scales with the peaks of recorded strong ground motion. Bull. of Seismological Soc. of Am. 65, 139–162.
Tuttle, M., Sweig, E., 1996. Recognizing and dating prehistoric liquefaction features: lessons learned in the New-Madrid seismic zone, central United States. J. Geophys. Res. 101, 6171–6178.
Whipple, K., 2004. Bedrock rivers and the geomorphology of active orogens. Annu. Rev. of Earth and Planetary Sci. 32, 151–185. doi:10.1146/annurev.earth.32.101802.
Wheeler, R., 2002. Distinguishing seismic from nonseismic soft-sediment structures: criteria from seismic hazard analysis. Geol. Soc. Am. Spec. Pap. 359, 1–11.
Wood, H.O., Neumann, F., 1931. Modified Mercalli intensity scale of 1931. Bull. of Seismological Soc. of Am. 21, 277–283.
Yonechi, F., 1976. The basin landforms in Nepal. Preprint Congr., Assoc. Japanese Geographers 11, 102–103 (in Japanese).
Yoshida, M., Igarashi, Y., 1984. Neogene to Quaternary lacustrine sediments in the Kathmandu Valley, Nepal. J. Nepal Geol. Soc. 4, 73–100.
Yoshida, M., Gautam, P., 1988. Magnetostratigraphy of Plio–Pleistocene lacustrine deposits in the Kathmandu valley, central Nepal. Proc. Indian. Nat. Sci. Acad. 54A, 410–417.
Yule, D., Dawson, S., Lave, J., Sapkota, S., Tiwari, D., Madden, C., 2007. Evidence for surface rupture of the Main Frontal Thrust during the great 1505 Himalayan earthquake, far-western Nepal. International Workshop on Investigation of Past Earthquakes in Nepal Himalaya. Paleoseismology, History and Archaeology, Kathmandu, Nepal. 2007.
Zhao, W., Nelson, K.D., project INDEPTH Team, 1993. Deep seismic reflection evidence for continental underthrusting beneath southern Tibet. Nature 366, 55–559.